

Received March 6, 2019, accepted March 27, 2019, date of publication April 4, 2019, date of current version April 16, 2019.

Digital Object Identifier 10.1109/ACCESS.2019.2909273

# Investigation of a Longitudinal and Lateral Lane-Changing Motion Planning Model for Intelligent Vehicles in Dynamical Driving Environments

HONGYU ZHENG<sup>1</sup>, JIAN ZHOU<sup>1</sup>, QIAN SHAO<sup>2</sup>, AND YULEI WANG<sup>1,3</sup>

<sup>1</sup>State Key Laboratory of Automotive Simulation and Control, Jilin University, Changchun 130022, China

<sup>2</sup>Department of Management Science and Engineering, Jilin University, Changchun 130022, China

<sup>3</sup>Department of Control Science and Engineering, Jilin University, Changchun 130022, China

Corresponding author: Yulei Wang (wangyulei@jlu.edu.cn)

This work was supported by the National Natural Science Foundation of China under Grant 51575223.

**ABSTRACT** This paper describes a lane-changing motion planning model for intelligent vehicles under constraints of collision avoidance in dynamical driving environments. The key innovation is decoupling the longitudinal and lateral motion planning to realize trajectory re-planning in a normal lane-changing process to prevent collisions. The longitudinal planning model decides a collision-free termination point of motion through planning the longitudinal acceleration and velocity. Taking the termination time as input, the lateral planning model plans the optimal reference trajectory for normal lane-changing maneuvers or re-plans the lane-changing trajectory to eliminate potential accidents. When traffic states have variations that may bring about the collisions, the termination point can be updated through the longitudinal planning model, based on which the lateral planning model makes adjustments to the pre-planned trajectory to complete the lane-changing successfully or return its original lane. The simulation results show that the proposed model not only can handle the general motion planning problem but also can re-plan trajectories in emergent conditions to ensure safety, while vehicle dynamics retain in a stable state during the lane-changing or returning maneuvers.

**INDEX TERMS** Intelligent vehicles, motion planning, accident prevention, optimization.

## I. INTRODUCTION

According to accident reports, human errors account for 90% of traffic accidents, among them, the lane-changing maneuver is the main factor for various crash accidents because of inaccurate estimation of traffic states, or illegal maneuvers [1], [2]. With the development of advanced sensing and control techniques, the intelligent vehicle is regarded as a solution to reduce the driver's workloads as well as increase driving safety [3]. Therefore, research efforts on the active lane-changing system have attracted increasing attentions from academia and industries.

A completely active lane-changing system has four modules: the sensory and communication module, the decision-making module, the motion planning module, and

The associate editor coordinating the review of this manuscript and approving it for publication was Fuhui Zhou.

the execution module [4]. Through the sensory and communication module, environmental information, including the road friction coefficient and lane marks are observed [5], [6]. And information among vehicles, including vehicle speeds and accelerations could be exchanged by vehicle-to-vehicle (V2V) communication systems [7], [8]. Based on such information, the decision-making module makes reasonable instructions [9], [10]. The motion planning module provides a feasible reference trajectory after receiving the lane-changing demand from the decision-making module [11]. And the execution module applies steering actions to make the vehicle follow the reference lane-changing trajectory [12].

This paper studies the motion planning strategy in the active lane-changing system of the intelligent vehicle, because the design has to take many constraints into consideration, such as collision avoidance and driving comfort, which are essential for intelligent vehicles to be accepted by

society [13]. This topic has been extensively investigated in literature, starting from the development of mobile robotics applications [14]. The most relevant vehicle lane-changing motion planning techniques in literature can be roughly divided into five categories, i.e., the graph search-based planner, the sampling-based planner, the interpolating curve planner, the numerical optimization planner, and the mechanism model-based planner [15].

In the graph search-based planner, the heuristic algorithms are often used. Yang *et al.* developed a modified Dijkstra algorithm to determine the shortest lane-changing path [16]. Madås *et al.* introduced the state lattice algorithm in vehicle automotive collision avoidance systems. The state lattice algorithm can be extended in some complex conditions with a proper planning precision [17]. The graph search-based planner is effective for planning a collision avoidance path when the obstacles are static and vehicle speed is not high. As a result, it is not applicable in dynamical traffic environments with moving obstacles.

One classical sampling-based path planning algorithm is the rapidly-exploring random tree (RRT) algorithm, which is suitable for planning obstacle avoidance paths for mobile robots. It can also be employed by the intelligent vehicle after some improvements. For instance, Lan and Cairano proposed a two-stage RRT algorithm to plan the safe lane-changing path of a semi-autonomous vehicle [18]. The RRT algorithm is able to provide a fast solution in real time. However, the path generated by RRT is jerky [19]. Therefore, this method is not widely used.

The interpolating curve planner is the most widely used lane-changing trajectory planning technique because it can take the vehicle dynamic and kinematic characteristics into account. It can be used to plan trajectories in some complex driving environments with moving obstacles and multi-lanes, or even in some emergent conditions. Presently, there are many standardized lane-changing trajectories in this planner. Mehdi *et al.* studied a collision avoidance algorithm based on piecewise Bézier curves, which could check for possible collisions with surrounding vehicles [20]. Zhu *et al.* applied a sinusoidal trajectory model in lane-changing assistance system to realize the personalized planning [21]. Schnelle *et al.* took the modified hyperbolic tangent function to generate the desired lane-changing path for the driver in a personalized driver steering model [22]. Besides, the hyperbolic tangent-based path was used by Suh *et al.* in a stochastic lane-changing decision system to limit the vehicle maximum lateral acceleration [23]. In the personalized driver steering model, Schnelle *et al.* also tried to use the spline as the path model [24]. In order to control the maximum curvature, the clothoid model and the trapezoid acceleration model were developed [25]. Funke and Gerdes presented a lane-changing model that integrated clothoid and circulars to obtain the real-time trajectory [26]. Soudbaksh *et al.* developed a trapezoid acceleration model to limit the maximum lateral acceleration of lane-changing [27]. In addition, the polynomial trajectory has also received extensive attention. Wang *et al.* employed

the cubic polynomial to plan the trajectory in a vehicle automatic lane-changing system [4]. Wang *et al.* used the quintic polynomial to generate the driver's desired trajectory in vehicle lane-changing maneuvers [7]. Do *et al.* proposed a two-segment lane-changing model for intelligent vehicles to mimic the human-driver, the quintic polynomial was used in the lateral model [28]. You *et al.* also applied the quintic polynomial trajectory in their studies [29]. The polynomial trajectory is very popular because the order of which can be tuned to achieve desired performances [30], [31]. The cubic polynomial trajectory has a smooth lateral velocity by setting the constant of its first derivative to 0, the quintic polynomial trajectory has a smooth curvature by setting constants of its first and second derivatives to 0, and the seven-order polynomial has a smooth jerk of lateral acceleration by setting constants of its first, second, and third derivatives to 0 [32]–[34].

The numerical optimization planner is often combined with other methods to find an optimal trajectory, such as the A \* algorithm [35] and the polynomial [36], therefore, a hierarchical planning architecture is often designed in this planner [37]. Lim *et al.* presented a hierarchical trajectory planning strategy for autonomous driving, the sampling-based approach was used at the behavior planning level and the optimization was conducted at the trajectory planning level [38]. Nilsson *et al.* selected inter-vehicle traffic gap and time instance as optimization variables in lane-changing maneuvers, they are solved by two convex quadratic programs [39]. Numerical optimization technique was also used by Li *et al.* to design the cooperative lane-changing strategy in the highway [40]. In this planner, constraints on vehicle dynamics and geometric elements can be considered to obtain the feasible results.

The mechanism model-based planner includes the artificial potential field (APF) algorithm and the driver model-based algorithm [41], [42]. Wolf and Burdick used APF to plan the lane-changing trajectory in a collision avoidance scenario [43]. Ji *et al.* constructed a 3-D virtual dangerous potential field in the vehicle collision avoidance system [44]. Zhou *et al.* proposed a lane-changing model from the driver's vision view [45], and Xu *et al.* developed a driver's lateral acceleration decision model to plan the lane-changing trajectory [46]. The APF algorithm generates the trajectory along the steepest potential gradient, but it cannot handle vehicle kinematic constraints. The driver model-based method can realize the personalized planning [47]. Nevertheless, to realize the personalized control based on planning is difficult because the driving style is changeable.

The aforementioned methods are summarized in Table 1 [15], [19], [48]. Conclusions from Table 1 show that these conventional techniques have their own applications. However, none of these researches are able to deal with a potential collision that arises in the lane-changing process of the vehicle in dynamical environments. When traffic states have variations that may bring about accidents, the subject vehicle needs to re-plan the reference trajectory

**TABLE 1.** Summarization of conventional lane-changing trajectory planning techniques.

Category	Technique	Description	Characteristic	Research
Graph search-based planner	Dijkstra algorithm	It searches for the shortest path in directed graphs with a set of weighted nodes/cells.	It is suitable for planning in static environments; the real-time performance is not good.	[16]
	State lattice	Defining the lattice accuracy and discretizing the space into a set of lattices at first, a cost function is then built to decide the best path.	It is able to handle multi-dimensions planning problems; the computation cost increases with lattice density; the trajectory cannot be re-planned.	[17]
Sampling-based planner	RRT	It searches for a collision-free trajectory on non-convex spaces by the space-filling tree, which is constructed from random samples.	The algorithm can be applied in multi-dimensional systems; it is suitable for global searching; the solution is applicable in dynamical environments.	[18]
Interpolating curve planner	B'ezier curves	Third-order or higher-order B'ezier curves can be used to plan lane-changing trajectories based on pre-determined points in the planning area.	The computation cost is low; the planning complexity increases with the degree; the trajectory cannot be re-planned in the lane-changing course.	[20]
	Sinusoidal curve	Setting the initial phase of the sinusoidal function to 0 and adjusting the amplitude and frequency of the function to get the trajectory.	The lateral acceleration can be planned directly; the curvature is smooth; the trajectory cannot be re-planned during the lane-changing process.	[21]
	The modified hyperbolic tangent function	Determining the termination time for lane-changing at first and then adjusting constants in the modified hyperbolic tangent function to obtain the desired lane-changing trajectory.	The planned trajectory has smooth and continuous lateral acceleration; the result is sensitive to model parameters; the trajectory cannot be re-planned during the lane-changing process.	[22],[23]
	Spline	Given a group of control points in the planning area beforehand, the lane-changing trajectory can be obtained by piecewise interpolation through the polynomial with different orders.	The computational cost is low; the trajectory is smooth and continued; the solution may not be optimal; the trajectory cannot be re-planned during lane-changing unless the spline model is modified.	[24]
	Clothoid or trapezoid acceleration	It generates lane-changing trajectory by clothoid and circular segments. The joint points are decided to make the curvature continued.	The lateral acceleration can be controlled directly through the clothoid; model parameters are complex; the trajectory cannot be re-planned.	[25], [26], [27]
	Polynomial	Determining the termination time for lane-changing at first, and then tuning the order of polynomial to obtain the trajectory with desired performance. The order of the polynomial should be greater than or equal to 3.	The computation cost of planning is low; the trajectory performance can be adjusted by tuning polynomial order; the curvature is smooth and continued; the trajectory cannot be re-planned when using the conventional polynomial model.	[4],[7], [28],[29], [30],[31], [32],[33], [34]
Numerical optimization planner	Function optimization	Constructing an optimization object according to the specific demand, and then designing suitable constraints to solve out the optimal parameters of the lane-changing trajectory.	Vehicle dynamics and geometric elements can be included; the optimization is usually conducted based on other planning methods; the result may not be optimal but feasible within the constraints.	[35],[36], [37],[38] [39],[40]
Mechanism model-based planner	APF	Establishing a gravitational field through the target point and a repulsive force field, then determining the motion direction of the vehicle.	The planned trajectory is smooth; the vehicle's safety depends heavily on the accuracy of the potential field; the trajectory cannot be re-planned.	[41], [42], [43]
	Driver model-based algorithm	A driver steering model is built beforehand, and the trajectory is planned by imitating the driver's lane-changing maneuver.	The personalized planning can be realized, but not suitable for the full-automatic driving scene; it is often used in combination with other planners.	[44],[45], [46],[47]

to prevent collisions. There are three steering scenarios for the subject vehicle: I. Surrounding vehicles do not pose threats to the subject vehicle, while the subject vehicle completes lane-changing normally. II. When there are potential collisions in the current environment, the subject vehicle needs to correct the pre-planned trajectory to accomplish lane-changing. III. When the normal and the corrected lane-changing schemes are all infeasible, the subject vehicle has to return to its starting lane. Therefore, it requires a method to realize trajectory re-planning in lane-changing course to ensure driving safety of the subject vehicle.

For conventional methods, reference trajectories are planned based on the assumption that the surrounding traffic states retain constant in the lane-changing period. As a result, the reference longitudinal termination points of lane-changing are fixed at the beginning, and these conventional techniques without dynamical correction abilities can only plan reference trajectories between two fixed

points. Starting from the limitations of these conventional approaches, this paper proposes a motion planning strategy that includes the longitudinal and lateral planning models. The longitudinal model determines the collision-free termination point in the current driving condition, this termination point can be updated according to specific traffic states, and the lateral model can plan a feasible trajectory from the vehicle's current position to the varying destinations. The main advantages of this approach over conventional planners are highlighted as follows:

1) The subject vehicle is able to correct the reference trajectory to accomplish lane-changing when surrounding vehicles change in accelerations or motion directions. Such variations may bring about collisions if the subject vehicle travels along the fixed reference trajectory.

2) The subject vehicle is able to return to its original lane when it perceives that the current lane-changing scheme is infeasible, and this scheme cannot be corrected to eliminate potential accidents.

This paper is organized as follows: Section II includes basic definitions and statements of this paper. Section III introduces the longitudinal motion planning model. In Section IV, the lateral motion planning model and trajectory optimization methods are presented. Section V builds the vehicle stability evaluation system to test the vehicle lane-changing performance. Section VI highlights the application of the proposed motion planning model in dynamical driving environments, comparisons are also conducted in this section. Section VII summarizes the paper.

## II. BASIC DEFINITIONS AND STATEMENTS

This research aims at planning trajectories for intelligent vehicles in dynamical traffic environments, as seen in Fig. 1.

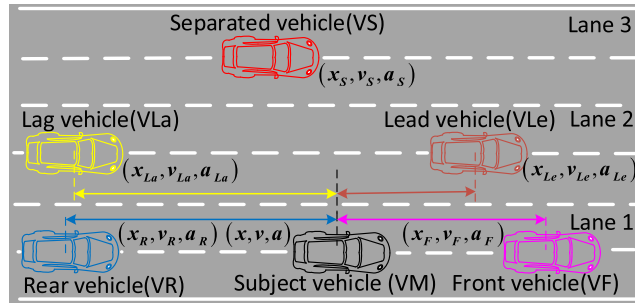


**FIGURE 1.** Model of the dynamical driving environment.

In Fig. 1, accelerations and motion directions of all vehicles may change by constituting a dynamical traffic environment. The original lane of the subject vehicle is lane 1, and the target lane is lane 2. Longitudinal accelerations, velocities, and positions of surrounding vehicles are obtained by the subject vehicle with the help of V2V technology. Based on such information, the planner decides the termination point, and then plans a reference lane-changing trajectory from the start position to the destination. During the normal lane-changing maneuver of the subject vehicle, there are two cases that may lead to trajectory re-planning. First, the lead vehicle decelerates, or the lag vehicle accelerates, and the subject vehicle would collide with them if it travels along the pre-planned trajectory. So the subject vehicle needs to correct the reference trajectory. Second, when the separated vehicle cuts into lane 2, the subject vehicle has to return as the trajectory of the separated vehicle is unpredictable. Based on the above analysis, some terms in this paper are defined as follows:

1) **The termination point:** it includes the longitudinal destination and the termination time of motion.

2) **Pre-planned trajectory:** it is the reference trajectory planned at first and relative to the re-planned trajectory.

3) **Normal lane-changing maneuver:** the subject vehicle completes lane-changing along the pre-planned trajectory without adjusting the termination point until the lane-changing finishes.

4) **Trajectory re-planning:** it includes the schemes of trajectory correction and trajectory reentry.

5) **Trajectory correction:** the vehicle adjusts the pre-planned termination point and plans a new trajectory in the

normal lane-changing process when it predicts collisions. The re-planned destination is still in the target lane, the vehicle can still accomplish lane-changing.

6) **Trajectory reentry:** the vehicle re-plans a reference trajectory from the current position to its starting lane when the normal lane-changing strategy and the corrected strategy are all infeasible.

The scenarios of the normal lane-changing, the trajectory correction, and the trajectory reentry are illustrated in Fig. 2. At first, the planner provides the normal reference trajectory for the subject vehicle, as shown in Fig. 2(a). When the subject vehicle predicts collisions in the normal lane-changing process, the longitudinal model re-plans a collision-free termination point through re-planning the longitudinal acceleration and velocity. Using this termination point as input,

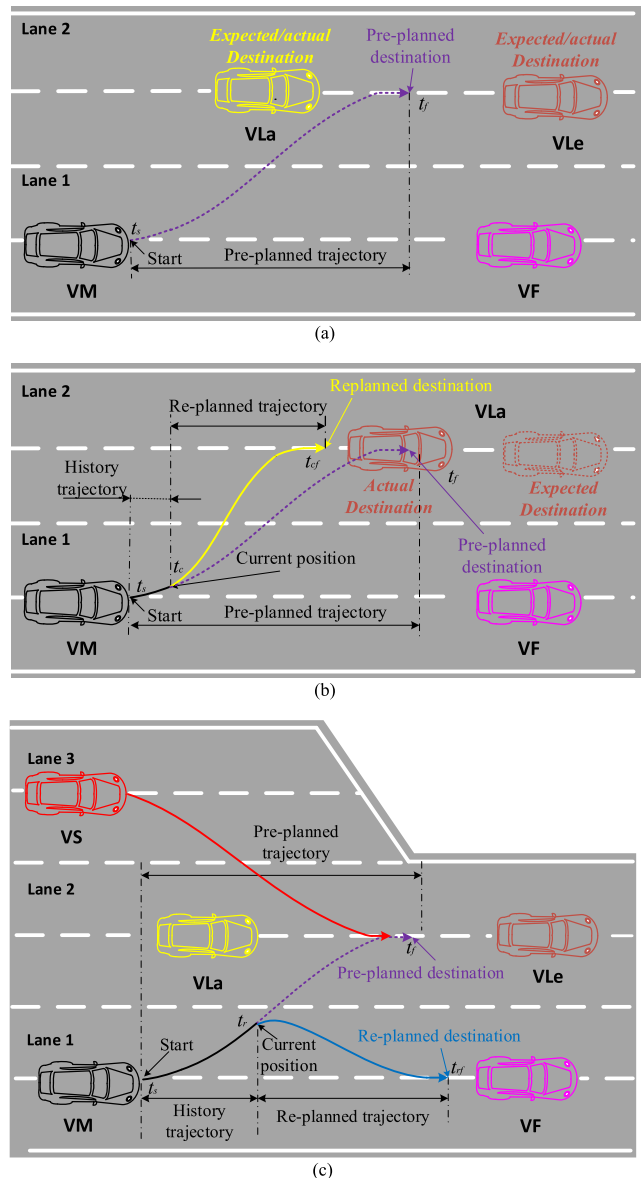


**FIGURE 2.** Typical steering scenarios of the subject vehicle: (a) Normal lane-changing. (b) Trajectory correction. (c) Trajectory reentry.

the lateral model re-plans a smooth reference trajectory for the vehicle to finish lane-changing, or return, as shown in Fig. 2(b) and Fig. 2(c), respectively. In the course of motion, the subject vehicle monitors surrounding traffic states in real time and feeds them back to the decision-making module, which makes. This paper focuses on the motion planning method, while the decision-making mechanism and the vehicle-to-vehicle communication technique are not within the research scope.

### III. LONGITUDINAL MOTION PLANNING MODEL

#### A. BASIC LONGITUDINAL MOTION PLANNING MODEL

The control input for vehicle in longitudinal is the longitudinal acceleration, which is adjusted by the opening of the throttle, or the pressure of the brake pedal [49]. Therefore, the longitudinal acceleration in the lane-changing process could be planned directly. By analyzing characteristics of longitudinal motions in previous researches [7], [25], this paper proposes a sinusoidal function-based model that decreases exponentially to plan the longitudinal acceleration in geodetic coordinates, i.e.,

$$a_x(t) = C \cdot e^{-A \cdot t} \cdot \sin\left(\frac{2\pi}{B} \cdot t\right), \quad (1)$$

where  $a_x(t)$  represents the longitudinal acceleration with time,  $A$ ,  $B$ , and  $C$  are model parameters,  $B > 0$ . Based on (1), the longitudinal velocity is planned as:

$$v_x(t) = v_{x0} + \int_0^t a_x(t) dt, \quad (2)$$

$$\int_0^t a_x(t) dt = -\frac{\alpha_1 + \alpha_2}{(A^2 \cdot B^2 + 4\pi^2)^2}, \quad (3)$$

with

$$\alpha_1 = B \cdot \left( 2\pi \cdot C \cdot e^{-At} \cdot \cos\left(\frac{2\pi t}{B}\right) + A \cdot \sin\left(\frac{2\pi t}{B}\right) \right),$$

$$\alpha_2 = 2\pi \cdot B \cdot C \cdot (A^2 \cdot B^2 + 4\pi^2),$$

where  $v_x(t)$  denotes the longitudinal velocity and  $v_{x0}$  is the initial value. Defining the longitudinal start position as  $x_0$ , the longitudinal displacement is planned as:

$$x(t) = x_0 + v_{x0} \cdot t + \int_0^t \int_0^t a_x(t) dt, \quad (4)$$

$$\int_0^t \int_0^t a_x(t) dt = \frac{B \cdot C \cdot (\beta_1 + \beta_2 + \beta_3)}{(A^2 \cdot B^2 + 4\pi^2)^2 \cdot e^{At}}, \quad (5)$$

with:

$$\beta_1 = (A^2 \cdot B^3 - 4\pi^2 \cdot B) \cdot \sin\left(\frac{2\pi t}{B}\right),$$

$$\beta_2 = (8\pi^3 \cdot t - 4\pi AB^2 + 2\pi \cdot t \cdot A^2 \cdot B^2) \cdot e^{At},$$

$$\beta_3 = 4\pi \cdot A \cdot B^2 \cdot \cos\left(\frac{2\pi t}{B}\right).$$

According to (1) and (2), the vehicle longitudinal motion characteristics affected by parameters  $A$ ,  $B$ , and  $C$  are illustrated in Fig. 3. In Fig. 3, peak values of longitudinal accelerations and velocities increase with the increase of  $A$ , and

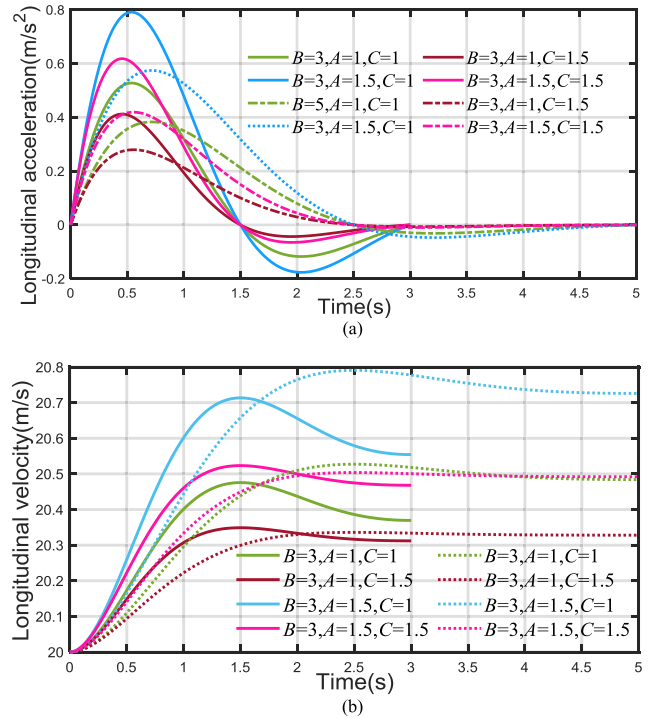


**FIGURE 3.** Longitudinal motion characteristics affected by model parameters: (a). Longitudinal acceleration. (b). Longitudinal velocity.

decrease with the increase of  $B$  and  $C$ . Fig. 3 shows that the longitudinal motion is smooth, which is good for driving experiences [50]. So the proposed longitudinal planning model has the potential to be applied in realistic.

#### B. TERMINATION TIME OF NORMAL TRAJECTORY

In the normal lane-changing maneuver, the longitudinal model determines the longitudinal destination and the lane-changing duration through planning longitudinal motions. In Fig. 1, the start time and initial longitudinal position of lane-changing are 0. Variables to be planned are  $A$ ,  $B$ , and  $C$ , which are solved from the following problem:

$$J = \min \left\{ w_1 \cdot \frac{D[a_x(t)]}{\hat{D}} + w_2 \cdot \left( \frac{\Delta x}{\hat{x}} \right)^2 + w_3 \cdot \left( \frac{\Delta v_{xLe}(t_f)}{\Delta \hat{v}_x} \right)^2 \right\}, \quad (6)$$

s.t.

$$\begin{cases} \left( x_F(t_{hf}) + L_F(0) + SD_{t_{hf}}^F \right) - \left( x(t_{hf}) + SD_{t_{hf}}^M \right) - \frac{l_{xF}}{2} > \hat{d}, \\ \left( x(t_{hf}) + L_R(0) + SD_{t_{hf}}^M \right) - \left( x_R(t_{hf}) + SD_{t_{hf}}^R \right) - \frac{l_{yM}}{2} > \hat{d}, \\ \left( x_{Le}(t_f) + L_{Le}(0) + SD_{t_f}^{Le} \right) - \left( x(t_f) + SD_{t_f}^M \right) - \frac{l_{yLe}}{2} > \hat{d}, \\ \left( x(t_f) + L_{La}(0) + SD_{t_f}^M \right) - \left( x_{La}(t_f) + SD_{t_f}^{la} \right) - \frac{l_{yM}}{2} > \hat{d}, \\ |a_x(t)| \leq a_{x \max}, \\ |\dot{a}_x(t)| \leq j_{x \max}, \\ A, C > 0, \\ 3 < B < 8, \end{cases}$$

with

$$\begin{aligned} t_{hf} &= \frac{t_f}{2}, \\ \Delta x &= x(t_f) - x(t_s), \end{aligned}$$

$E[a_x(t)]$

$$= \frac{\int_{t_s}^{t_f} a_x(t) dt}{t_f - t_s},$$

$\Delta v_{xLe}^x(t_f)$

$$= v_x(t_f) - v_{xLe}(t_f),$$

$v_{xR}(t_{hf})$

$$= v_{xR}(t_s) + \int_{t_s}^{t_{hf}} a_{xR}(t) dt,$$

$v_{xLa}(t_f)$

$$= v_{xLa}(t_s) + \int_{t_s}^{t_f} a_{xLa}(t) dt,$$

$x_F(t_{hf})$

$$= v_{xF}(t_s) \cdot t + \int_{t_s}^{t_{hf}} \int_{t_s}^{t_{hf}} a_{xF}(t) dt,$$

$x_R(t_{hf})$

$$= v_{xR}(t_s) \cdot t + \int_{t_s}^{t_{hf}} \int_{t_s}^{t_{hf}} a_{xR}(t) dt,$$

$x_{Le}(t_f)$

$$= v_{xLe}(t_s) \cdot t + \int_{t_s}^{t_f} \int_{t_s}^{t_f} a_{xLe}(t) dt,$$

$x_{La}(t_f)$

$$= v_{xLa}(t_s) \cdot t + \int_{t_s}^{t_f} \int_{t_s}^{t_f} a_{xLa}(t) dt,$$

$D[a_x(t)]$

$$= \frac{\int_0^{t_f} (a_x(t))^2 dt - 2E(a_x(t)) \cdot \int_0^{t_f} a_x(t) dt + E(a_x(t))^2}{t_f - t_s},$$

where  $t_s$  is the start time of lane-changing,  $t_f$  is the termination time of lane-changing. In (6), the first target is to minimize the variance of longitudinal acceleration, the second target is to limit the maximum longitudinal displacement, and the last target is to minimize the error between the subject vehicle and the lead vehicle in the target lane, as the driver usually hopes to decrease this error when lane-changing finishes [31].  $w_1$ ,  $w_2$ , and  $w_3$  are weights of three targets,  $\hat{D}$  is the standard variance of longitudinal acceleration,  $\hat{x}$  is the standard longitudinal displacement,  $\Delta \hat{v}_x$  is the standard speed difference.  $v_{xF}(t)$ ,  $v_{xR}(t)$ ,  $v_{xLe}(t)$ ,  $v_{xLa}(t)$  represent the longitudinal velocity of the front vehicle, the rear vehicle, the lead vehicle, and the lag vehicle, respectively.  $a_{xF}(t)$ ,  $a_{xR}(t)$ ,  $a_{xLe}(t)$ , and  $a_{xLa}(t)$  indicate the longitudinal acceleration of the front vehicle, the rear vehicle, the lead vehicle, and the lag vehicle, respectively.  $v_x(t_{hf})$  and  $x(t_{hf})$  are calculated by bringing  $t_{hf}$  into (2) and (4), respectively, as well as solutions of  $v_x(t_f)$  and  $x(t_f)$ .  $L_F(t_s)$ ,  $L_a(t_s)$ ,  $L_{Le}(t_s)$ , and  $L_{La}(t_s)$  mean

the longitudinal distance between the subject vehicle and surrounding vehicles at the start.  $l_{vM}$  denotes the length of the subject vehicle,  $l_{vF}$  and  $l_{vLe}$  denote the length of the front vehicle and the lead vehicle, respectively.  $\hat{d}$  is the standard safe distance.  $a_{xmax}$  is the threshold of longitudinal acceleration, and  $j_{xmax}$  is the threshold of longitudinal jerk.  $SD$  is the stopping sight distance [51], e.g., for the subject vehicle, the stopping sight distance at  $t_f$  is calculated as:

$$SD_{t_f}^M = \frac{v_x(t_f)^2}{19.6 \times (\mu \pm f)} + t_p \cdot v_x(t_f) \cdot 0.278, \quad (7)$$

where  $\mu$  is the road friction coefficient,  $f$  is the grade of  $\mu$ , and  $t_p$  is a perception-reaction time. The remaining stopping sight distances in (6) are calculated by the same method.

In (6), the first two constraints ensure the subject vehicle maintains a safe distance with the front vehicle and the rear vehicle in the lane-changing period. The third and fourth constraints ensure a safe terminal position of the subject vehicle in the target lane [52]. However, it is quite difficult to obtain the global optimal solution as (6) is a multivariate nonlinear optimization problem. Considering that there is no equality constraint, the interior penalty function (IPF) algorithm is recommended to deal with such problem [53]. In the IPF algorithm, the penalty function is constructed as:

$$\varphi(R, r^{(k)}) = J(R) - r^{(k)} \sum_{i=1}^9 \ln [g_i(R)], \quad (8)$$

where  $R = \{A, B, C\}$ ,  $r^{(k)}$  is the penalty factor, and  $k$  means iteration times, which belongs to a decreasing sequence, i.e.,

$$r^{(k)} = C \cdot r^{(k-1)}, \quad 0 < C < 1, \quad (9)$$

In (8),  $g_i(R)$  represents the set of inequality constraints, for instance,  $g_5(R)$  is expressed as:

$$g_5(R) = a_{xmax} - |a_x(t)| \geq 0 \quad (10)$$

The iteration termination criteria is defined as:

$$\left| r^{(k)} \sum_{i=1}^9 \ln |g_i(R)| \right| \leq \varepsilon. \quad (11)$$

where  $\varepsilon$  is the allowable iteration error. The IPF algorithm is detailed in Algorithm 1. After solving this optimization problem, the termination time of normal lane-changing is:

$$t_f = B + t_s. \quad (12)$$

### C. TERMINATION TIME OF CORRECTED TRAJECTORY

Trajectory correction is needed when the pre-planned lane-changing scheme is thwarted by collisions, defining  $t_c$  as the start time and  $t_{cf}$  as the termination time of the corrected trajectory, the longitudinal acceleration is re-planned as:

$$a_{cx}(t) = a_x(t_c) - C_c \cdot e^{-A_c \cdot (t-t_c)} \cdot \sin \left( \frac{2\pi \cdot (t-t_c)}{B_c} \right), \quad (13)$$

**Algorithm 1** The IPF Algorithm

---

**Data:**  $r^{(0)}$ ,  $\{A^{(0)}, B^{(0)}, C^{(0)}\}, C, k_{max}, \varepsilon, J(R), g_i(R)$

**Result:**  $R^{(opt)} = \{A^{(opt)}, B^{(opt)}, C^{(opt)}\}$

1. **Initialization:**  $r^{(0)} > 0, R^{(0)} = \{A^{(0)}, B^{(0)}, C^{(0)}\}, k = 0, \varepsilon > 0$
2. **while**  $k < k_{max}$  **do**
3.      $\{A^{(k)}, B^{(k)}, C^{(k)}\} = \min_R \varphi(R^{(0)}, r^{(k)})$
4.     **if**  $|r^{(k)} \sum_{i=1}^9 \ln |g_i(R)|| \leq \varepsilon$
5.         **return**  $\{A^{(opt)}, B^{(opt)}, C^{(opt)}\} = \{A^{(k)}, B^{(k)}, C^{(k)}\};$   
           **break**
6.     **else**
7.          $r^{(k+1)} = C \bullet r^{(k)}, R^{(0)} = \{A^{(k)}, B^{(k)}, C^{(k)}\}, k = k+1$
8.     **end**
9. **end**

---

with  $t \in [t_c, t_{cf}]$ , where  $a_{cx}(t)$  is the re-planned longitudinal acceleration during the correcting period,  $A_c$ ,  $B_c$ , and  $C_c$  are model parameters. Based on (13), the longitudinal velocity and the displacement during the correcting period are calculated as:

$$v_{cx}(t) = v_x(t_c) + \int_{t_c}^{t_c + B_c} a_{cx}(t) dt, \quad (14)$$

$$x_c(t) = x(t_c) + \int_{t_c}^{t_c + B_c} v_{cx}(t) dt. \quad (15)$$

In Fig. 2(b), variations of surrounding traffic states will bring psychological burden to the driver in the subject vehicle. So, the driver usually hopes to arrive in the target lane as soon as possible. In addition, it need not consider the front and rear vehicles when correcting the trajectory. As a consequent, the optimization object with its constraints in the trajectory correction scenario are built as follows:

$$J = \min \left\{ w_1 \cdot \left( \frac{\Delta x_c}{\hat{x}} \right)^2 + w_2 \cdot \left( \frac{\Delta v_{cx}^{xLe}(t_{cf})}{\Delta \hat{v}_x} \right)^2 \right\}, \quad (16)$$

s.t.

$$\begin{cases} X(L_e, t_{cf}) - (x_c(t_{cf}) - x(t_c) + SD_{t_{cf}}^M) - \frac{l_{vL_e}}{2} > \hat{d}, \\ (x_c(t_{cf}) - x(t_c) + SD_{t_{cf}}^M) - X(L_a, t_{cf}) + \frac{l_{vM}}{2} > \hat{d}, \\ |a_{cx}(t)| \leq a_{cx} \text{ max}, \\ |\dot{a}_{cx}(t)| \leq j_{cx} \text{ max}, \\ A_c, C_c > 0, \\ 1 < B_c < t_f - t_c, \end{cases}$$

with:

$$\begin{aligned} \Delta x_c &= x_c(t_{cf}) - x(t_c), \\ \Delta v_{cx}^{xLe}(t_{cf}) &= v_{cx}(t_{cf}) - v_{xLe}(t_{cf}), \\ v_{xLe}(t_{cf}) &= v_{xLe}(t_c) + \int_{t_c}^{t_{cf}} a_{xcLe}(t) dt, \\ v_{xLa}(t_{cf}) &= v_{xLa}(t_c) + \int_{t_c}^{t_{cf}} a_{xcLa}(t) dt, \end{aligned}$$

$$\begin{aligned} X(L_e, t_{cf}) &= v_{xLe}(t_c) \cdot t + \int_{t_c}^{t_{cf}} \int_{t_c}^{t_{cf}} a_{xcLe}(t) dt \\ &\quad + L_{Le}(t_{cf}) + SD_{t_{cf}}^{Le}, \end{aligned}$$

$$\begin{aligned} X(L_a, t_{cf}) &= v_{xLa}(t_{cf}) \cdot t + \int_{t_c}^{t_{cf}} \int_{t_c}^{t_{cf}} a_{xcLa}(t) dt \\ &\quad + SD_{t_{cf}}^{la} + L_{La}(t_{cf}), \end{aligned}$$

where  $a_{xcLe}$  and  $a_{xcLa}$  denote longitudinal accelerations of the lead and lag vehicles in the correcting period of the subject vehicle, respectively.  $a_{cxmax}$  is the updated threshold of longitudinal acceleration, and  $j_{cxmax}$  is the updated threshold of longitudinal jerk.  $SDLe$ ,  $SDM$ ,  $tcf$ , and  $SDLa$ ,  $tcf$  are computed by a similar method in (7). As (16) is a multivariate nonlinear optimization problem, it also needs to be solved by the IPF algorithm, as shown in (8)-(11), which not be repeated here.

After solving problem (16), the termination time for the re-planned trajectory is updated as:

$$t_{cf} = t_c + B_c. \quad (17)$$

**D. TERMINATION TIME OF RETURNED TRAJECTORY**

Trajectory reentry is another case of re-planning. Defining  $t_r$  as the start time of reentry, and  $t_{rf}$  as the new termination time, the longitudinal acceleration in the reentry process is:

$$a_{rx}(t) = a_x(t_r) + C_r \cdot e^{-A_r \cdot (t - t_r)} \cdot \sin \left( \frac{2\pi \cdot (t - t_r)}{B_r} \right), \quad (18)$$

with  $t \in [t_r, t_{rf}]$ , where  $a_{rx}(t)$  is the re-planned longitudinal acceleration,  $A_r$ ,  $B_r$ , and  $C_r$  are parameters. Longitudinal velocity ( $v_{rx}(t)$ ) and displacement ( $x_r(t)$ ) are re-planned as:

$$v_{rx}(t) = v_x(t_r) + \int_{t_r}^{t_{rf}} a_{rx}(t) dt, \quad (19)$$

$$x_r(t) = x(t_r) + \int_{t_r}^{t_{rf}} v_{rx}(t) dt. \quad (20)$$

During the returning period, the subject vehicle only needs to avoid collisions with the front vehicle and the rear vehicle, so model parameters are solved from the following problem:

$$J = \min \left\{ w_1 \cdot \left( \frac{\Delta x_r}{\hat{x}} \right)^2 + w_2 \cdot \left( \frac{\Delta v_{rx}^{xLe}(t_{rf})}{\Delta \hat{v}_x} \right)^2 \right\}, \quad (21)$$

s.t.

$$\begin{cases} X(F, t_{rf}) - (x_r(t_{rf}) - x(t_{rt}) + SD_{t_{rf}}^M) - \frac{l_{vF}}{2} > \hat{d}, \\ (x_r(t_{rf}) - x(t_{rt}) + SD_{t_{rf}}^M + L_R(t_{rf})) - X(R, t_{rf}) - \frac{l_{vM}}{2} > \hat{d}, \\ |a_{rx}(t)| \leq a_{rx} \text{ max}, \\ |\dot{a}_{rx}(t)| \leq j_{rx} \text{ max}, \\ A_r > 0, C_r < 0, \\ 1 < B_r < t_f - t_r, \end{cases}$$

with

$$\begin{aligned}\Delta x_r &= x_r(t_{rf}) - x(t_r), \\ \Delta v_{rx}^{xLe}(t_{rf}) &= v_{rx}(t_{rf}) - v_{xLe}(t_{rf}), \\ v_{xF}(t_{rf}) &= v_{xF}(t_r) + \int_{t_r}^{t_{rf}} a_{xF}(t) dt, \\ v_{xR}(t_{rf}) &= v_{xR}(t_r) + \int_{t_r}^{t_{rf}} a_{xR}(t) dt, \\ X(F, t_{rf}) &= v_{xF}(t_r) \cdot t + \int_{t_r}^{t_{rf}} \int_{t_r}^{t_{rf}} a_{xF}(t) dt + L_F(t_{rf}) + SD_{t_{rf}}^F, \\ X(R, t_{rf}) &= v_{xR}(t_r) \cdot t + \int_{t_r}^{t_{rf}} \int_{t_r}^{t_{rf}} a_{xR}(t) dt - L_R(t_{rf}) + SD_{t_{rf}}^R,\end{aligned}$$

where  $a_{xF}$  and  $a_{xR}$  are longitudinal accelerations of the front and rear vehicles during the reentry process of the subject vehicle, respectively.  $a_{rxmax}$  is an updated threshold of longitudinal acceleration,  $j_{rxmax}$  is an updated threshold of longitudinal jerk. Stopping distances are computed by similar formulas in (7). Similarly, (21) is solved by the IPF algorithm, then the updated termination time for reentry is:

$$t_{lf} = t_r + B_r. \quad (22)$$

## IV. LATERAL MOTION PLANNING MODEL

### A. NORMAL LANE-CHANGING TRAJECTORY

Table 1 shows some classical trajectory planning models. Among them, the polynomial, the sinusoidal curve, the hyperbolic tangent function, and the trapezoid acceleration model are widely used [21], [23], [27], [31]. Lane-changing trajectories generated by these four models are in Fig. 4.

Fig. 4(a)–(b) shows that the quintic polynomial and the sinusoidal curve can only plan one trajectory given a destination. This trajectory may not be optimal as it is not optimized from a cluster. Fig. 4(c) reveals that most of trajectories generated by the hyperbolic tangent function are not suitable for lane-changing. And Fig. 4(d) indicates that there are too many undermined parameters in the trapezoid acceleration model. Therefore, this research introduces a model that can generate trajectories from the start to the destination. This model is derived from the driver's lateral acceleration decision mechanism in the steering process [46], with the preliminary model expressed as:

$$\begin{cases} \dot{e}_y(t) = p \cdot (w - e_y(t)) + q \cdot \dot{e}_y(t) \\ e_y(t_s) = 0, \dot{e}_y(t_s) = 0, t_s = 0 \end{cases}, \quad (23)$$

where  $e_y(t)$  means the lateral displacement in geodetic coordinates,  $w$  is the target lateral destination,  $p$  and  $q$  are model parameters, the range of which can be calculated by Laplace transform of (23), i.e.,

$$\frac{1}{e_y(s)} = \frac{p \cdot w}{s \cdot \left( s - \frac{q+\sqrt{q^2-4p}}{2} \right) \cdot \left( s - \frac{q-\sqrt{q^2-4p}}{2} \right)}. \quad (24)$$

The above transfer function is stable when  $q < 0$ ,  $p > 0$ , and  $q^2-4p < 0$ . Then the lateral velocity is derived

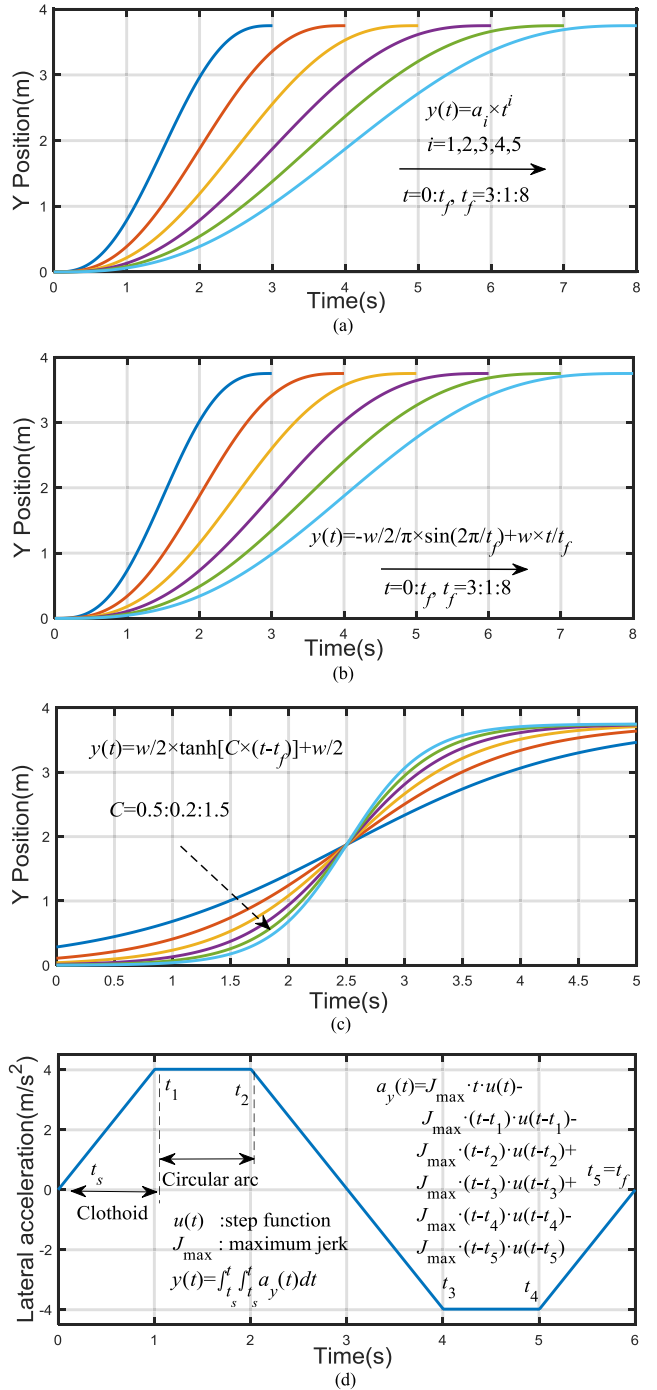


**FIGURE 4.** Generated lane-changing trajectories by conventional models:  
(a) Quintic polynomial. (b) Sinusoidal curve. (c) Hyperbolic tangent function. (d) Clothoid or trapezoid acceleration model.

from (23), i.e.,

$$\dot{e}_y(t) = \frac{2p \cdot w \cdot \sin\left(\frac{\sqrt{4p-q^2}}{2} \cdot t\right)}{\sqrt{4p-q^2} \cdot e^{-\frac{q}{2} \cdot t}}, \quad (25)$$

In (25), the lateral velocity of the vehicle is zero at the start, and it also requires the lateral velocity be zero at the

termination point. As a result, the second zero of (25) is ought to be determined as the termination time, i.e.,

$$t_f = \frac{2\pi}{\sqrt{4p - q^2}}. \quad (26)$$

Notice that the vehicle should arrive in the target lane at  $t_f$ , on the basis of the preliminary model in (23), the lateral displacement in the lane-changing process is derived as:

$$y(t) = k_1(p, q) \cdot \int_0^{t_f} \dot{e}_y(t) dt, \quad (27)$$

with terminal constraint as  $y(t_f) = w$ .  $k_1(p, q)$  is the coefficient to satisfy the terminal constraint. Bring in the terminal constraint, (27) is rewritten as:

$$y(t) = k_1(p, q) \cdot \left( 1 - e^{\frac{q}{2} \cdot t} \cdot A_1 \cdot \sin(A_2 \cdot t - \arctan A_3) \right), \quad (28)$$

$$k_1(p, q) = \frac{w^2}{\int_0^{t_f} \dot{e}_y(t) dt}, \quad (29)$$

with

$$A_1 = \sqrt{\frac{4p}{4p - q^2}}, A_2 = \sqrt{\frac{4p - q^2}{2}}, A_3 = \frac{q}{\sqrt{4p - q^2}}.$$

In (26),  $t_f$  is the function of  $p$  and  $q$ . When  $t_f$  is given in (12), a trajectory cluster is generated by tuning  $p$  and  $q$ , as given in Fig. 5. Trajectories in Fig. 5 are all suitable for lane-changing. Different trajectories in the cluster have different performances, which provides the opportunity to select the optimal one. Usually, the driver is more sensitive to the lateral motion when steering [29]. Accordingly, the optimization can be designed with the aim of finding the trajectory with the smallest peak of lateral acceleration. According to (27), the lateral acceleration is expressed as:

$$a_y(t) = \frac{w \cdot p \cdot e^{\frac{q}{2} \cdot t} \cdot A_1 \cdot \sin\left(\frac{A_2}{\sqrt{2}} \cdot t + \frac{1}{A_3}\right)}{1 - e^{\frac{q}{2} \cdot t_f} \cdot A_1 \sin(A_2 \cdot t_f - \arctan A_3)}, \quad (30)$$

with

$$A_1 = \sqrt{\frac{4p}{4p - q^2}}, A_2 = \sqrt{\frac{4p - q^2}{2}}, A_3 = \frac{q}{\sqrt{4p - q^2}}.$$

Peak times of  $a_y(t)$  are calculated from the first derivation of (30), which are expressed as:

$$t_{p1} = 0, t_{p2} = \frac{2 \left( \pi - \arctan \frac{q \cdot \sqrt{4p - q^2}}{q^2 - 4p} \right)}{\sqrt{4p - q^2}}, \quad (31)$$

where  $t_{p1}$  and  $t_{p2}$  are peak times of the lateral acceleration. Then, the optimization object is constructed as:

$$J = \min \{ |w_1 \cdot a_y(t_{p1})| + |w_2 \cdot a_y(t_{p2})| \}, \quad (32)$$

s.t.

$$\begin{cases} 0 < p < 10, -10 < q < 0, q^2 - 4p \leq 0, \\ \frac{2\pi}{\sqrt{4p - q^2}} - t_f = 0. \end{cases}$$

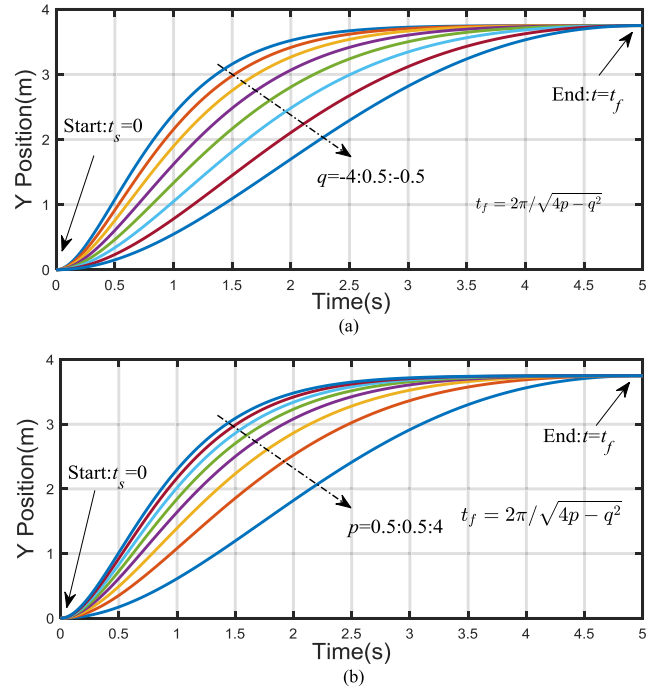


**FIGURE 5.** Generated trajectory cluster by tuning model parameters  $p$  and  $q$ : (a) Tuning  $q$ , (b) Tuning  $p$ .

where  $w_1$  and  $w_2$  are weight coefficients,  $t_f$  is decided in (12),  $p$  and  $q$  are variables to be solved, (32) is not as complex as (6), (16), and (21). So,  $p$  and  $q$  can be solved by the **fmincon** function in MATLAB [54], [55], the optimization result is shown in Fig. 6. It follows from Fig. 6 that the optimized lateral acceleration is smoother. However, it has jerks at the start and end points. Therefore, the result needs to be modified. Taking the preliminary optimized trajectory as the baseline, the function approximation method is utilized to modify the trajectory. The total number of hard constraints of the trajectory is six, so the approximation function should have at least seven degrees-of-freedom to design the approximation criteria. In order to avoid the Runge phenomenon, the six-order polynomial is applied, which is expressed in (33).

$$Y(t) = \sum_{i=0}^6 (a_i \cdot t^i), t \in [0, t_f] \quad (33)$$

where  $Y(t)$  is the function used for approximation, as well as the final expression of the lane-changing trajectory.  $a_0, \dots, a_6$  are coefficients. Defining the preliminary optimized trajectory as  $y_{opt}(t)$ , the approximation criteria is:

$$J = \min \left\{ \int_{t_s}^{t_f} (Y(t) - y_{opt}(t)) dt \right\}, \quad (34)$$

s.t.

$$\begin{cases} Y(0) = 0, \dot{Y}(0) = 0, \ddot{Y}(0) = 0, \\ Y(t_f) = w, \dot{Y}(t_f) = 0, \ddot{Y}(t_f) = 0. \end{cases}$$

Coefficients of the six-order polynomial in (33) are obtained by solving (34) through the **fmincon** function in MATLAB.

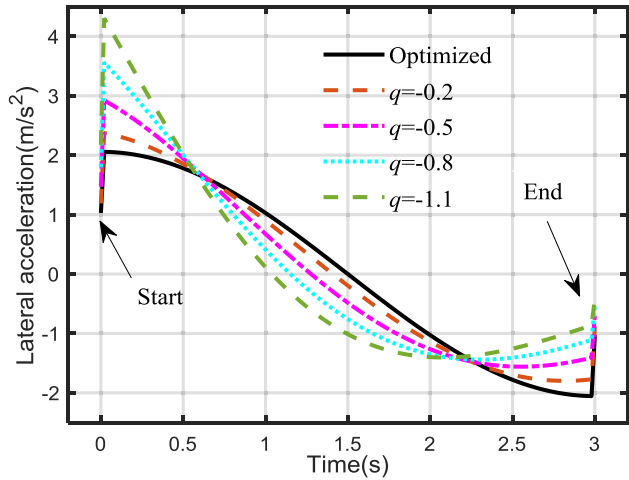


**FIGURE 6.** Comparisons of lateral accelerations before and after optimization with trajectories come from the cluster in Fig. 5.

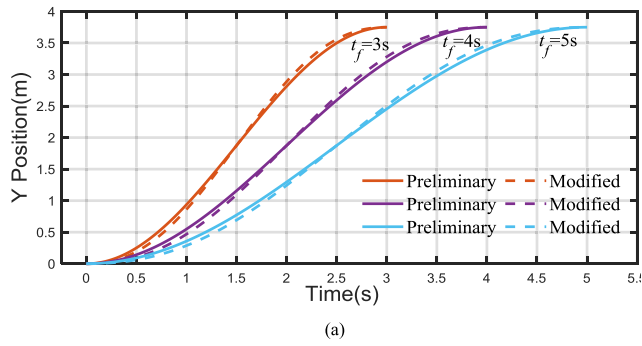


**FIGURE 7.** Comparisons of the preliminary trajectories and modified trajectories: (a). Trajectories. (b). Lateral accelerations.

To verify the modification effect, the preliminary trajectories and the modified results, as well as lateral accelerations are compared with  $t_f$  as 3s, 4s, and 5s, respectively, as shown in Fig. 7.

Fig. 7 describes that lateral accelerations of modified trajectories are improved. In addition, comparisons of lane-changing performances along the modified trajectories and quintic polynomial trajectories are presented in Fig. 8. In Fig. 8, lateral accelerations and yaw rates of modified trajectories are smoother and have lower peak values than those of quintic polynomial trajectories, which implies that

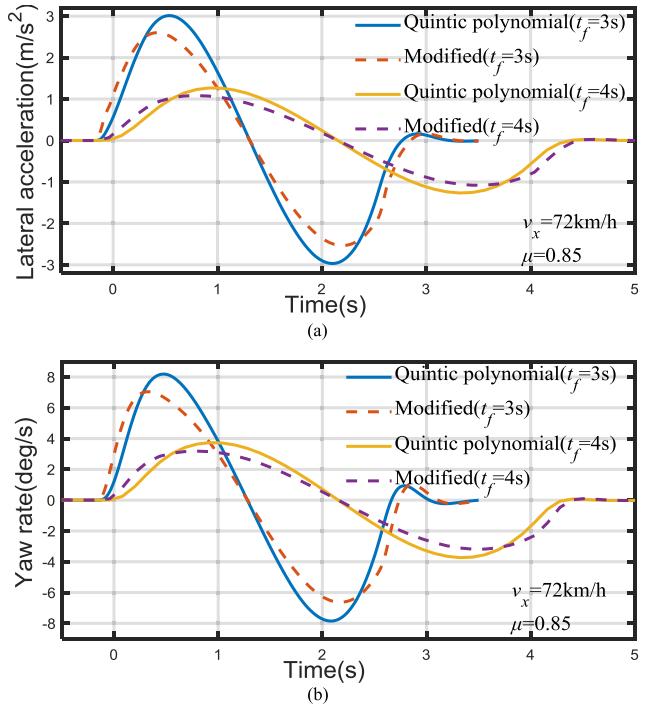


**FIGURE 8.** Comparisons between quintic polynomial trajectories and the modified trajectories: (a). Lateral acceleration. (b). Yaw rate.

the driver would feel more comfortable. These results reflect advantages of the proposed lateral planning model.

## B. TRAJECTORY CORRECTION

The termination time for trajectory correction is updated in (17) by the longitudinal planning model. In the lateral planning model, to correct the pre-planned trajectory, the initial conditions of (23) are changed as:

$$e_y(0) = Y(t_c), \dot{e}_y(0) = \dot{Y}(t_c). \quad (35)$$

Combing (23) and (35), the first derivative of  $e_y(t)$  is:

$$\dot{e}_y(t) = e^{\frac{q}{2} \cdot (t-t_c)} \cdot \sqrt{\gamma^2 + \dot{Y}(t_c)^2} \cdot \sin \left( \frac{A_2}{\sqrt{2}} \cdot (t-t_c) + \varphi \right), \quad (36)$$

with

$$A_2 = \frac{\sqrt{4p - q^2}}{2}, \gamma = \frac{q \cdot \dot{Y}(t_c) - 2p \cdot Y(t_c) + 2p \cdot w}{\sqrt{4p - q^2}},$$

$$\varphi = \arctan \frac{\sqrt{4p - q^2} \cdot \dot{Y}(t_c)}{2p \cdot w - 2p \cdot Y(t_c) + q \cdot \dot{Y}(t_c)}.$$

The lateral velocity should be zero when the vehicle arrives in the target lane, consequently, the zero of (36) is determined as the termination time of the corrected lane-changing maneuver, i.e.,

$$t_{cf} = \frac{2 \left( \pi - \arctan \left( \frac{\sqrt{4p - q^2} \cdot \dot{Y}(t_c)}{2p \cdot w - 2p \cdot Y(t_c) + q \cdot \dot{Y}(t_c)} \right) \right)}{\sqrt{4p - q^2}} + t_c, \quad (37)$$

Similar to (27), the corrected trajectory is preliminarily planned as:

$$y_c(t) = k_2(p, q) \cdot \int_{t_c}^{t_{cf}} \dot{e}_y(t) dt, \quad (38)$$

with the terminal constraint as  $y(t_{cf}) = w$ , which is satisfied by  $k_2(p, q)$ . The expansion of (38) is expressed as:

$$y_c(t) = \frac{w^2 \cdot \left(1 - e^{\frac{q}{2} \cdot (t-t_c)} \cdot \delta_1 + e^{\frac{q}{2} \cdot t} \cdot \delta_2 \cdot \delta_3\right)}{\int_{t_c}^{t_{cf}} \dot{e}_y(t) dt}, \quad (39)$$

with

$$\begin{aligned} \delta_1 &= \sqrt{\frac{16p - 3q^2}{4p - q^2}} \cdot \sin\left(\frac{A_2}{2}(t - t_c) + \varphi_1\right), \\ \delta_2 &= \sqrt{\left(\frac{4[\dot{Y}(t_c) - q \cdot Y(t_c)]}{\sqrt{4p - q^2}}\right)^2 + 4Y(t_c)^2}, \\ \delta_3 &= \sin\left(\frac{A_2}{\sqrt{2}} \cdot (t - t_c) + \varphi_2\right), \\ A_2 &= \frac{\sqrt{4p - q^2}}{2}, \\ \varphi_1 &= \arctan \frac{2\sqrt{4p - q^2}}{q}, \\ \varphi_2 &= \arctan \frac{Y(t_c) \cdot \sqrt{4p - q^2}}{2(\dot{Y}(t_c) - q \cdot Y(t_c))}. \end{aligned}$$

In (39), a trajectory cluster is generated by tuning  $p$  and  $q$  when  $t_{cf}$  is given in (17). A similar method in (32) could be employed to choose the optimal trajectory. However, since the expression of  $t_{cf}$  is a transcendental function, the optimization object in (32) cannot be established. As a result, the searching-based optimization method is applied.  $t_{cf}$  can be larger or smaller than  $t_f$ , the contour map of  $t_{cf}$  with  $p$  and  $q$  is shown in Fig. 9 when  $t_{cf}$  is smaller than  $t_f$ . In Fig. 9, when  $t_{cf}$  is decided, the corresponding contour line is determined,

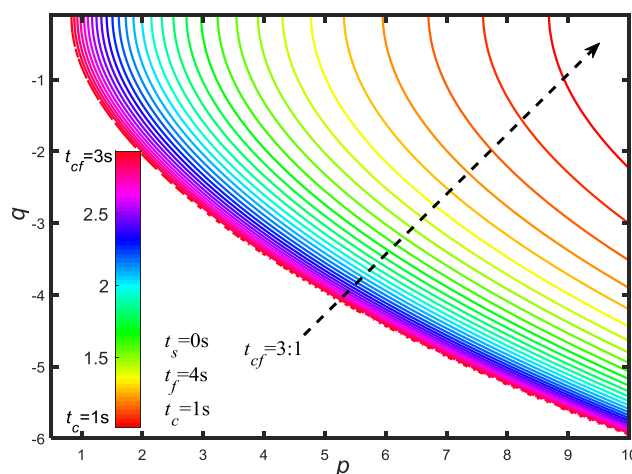


**FIGURE 9.** Contour map of  $t_{cf}$  with  $p$  and  $q$ .

trajectory parameters  $p$  and  $q$  are distributed on this contour line. Then the pair of parameters that determines the optimal trajectory can be found in this contour line according to the following criteria:

$$M(p, q) = \arg \min \{w_1 \cdot |\max[\ddot{y}_c(t)]| + w_2 \cdot |\min[\ddot{y}_c(t)]|\}_i, \quad (40)$$

with  $t \in [t_c, t_{cf}]$ ,  $M(p, q) \in [P_{tcf}, Q_{tcf}]$ .  $M(p, q)$  is the pair of  $p$  and  $q$  that generates the optimal trajectory,  $[P_{tcf}, Q_{tcf}]$  is the set of  $p$  and  $q$  in the contour line determined by  $t_{cf}$ . The preliminary optimized trajectory is defined as  $y_{c,opt}$ . However, the lateral acceleration of this trajectory also has jerks, which is similar to the condition in Fig. 6, and the trajectory needs to be modified by function approximation. The polynomial used for approximation is expressed as:

$$Y_c(t) = \sum_{i=0}^6 (a_{ci} \cdot t^i), \quad t \in [t_c, t_{cf}] \quad (41)$$

where  $Y_c(t)$  denotes the final expression of the corrected trajectory, as well as the function used for approximation.  $a_{c0}, \dots, a_{c6}$  are coefficients of the six-order polynomial, which are decided from the following optimization:

$$\begin{aligned} J &= \min \left\{ \int_{t_c}^{t_{cf}} (Y_c(t) - y_{c,opt}(t))^2 dt \right\}, \\ \text{s.t.} \\ \begin{cases} Y_c(t_c) = Y(t_c), \dot{Y}_c(t_c) = \dot{Y}(t_c), \ddot{Y}_c(t_c) = \ddot{Y}(t_c), \\ Y_c(t_{cf}) = w, \dot{Y}_c(t_{cf}) = 0, \ddot{Y}_c(t_{cf}) = 0. \end{cases} \end{aligned} \quad (42)$$

As (42) is a simple optimization problem with the only linear equality constraints, the polynomial coefficients can be solved by the `fmincon` function. Then the corrected trajectories and the pre-planned trajectory, as well as lateral accelerations are compared in Fig. 10 when  $t_f$  is 5s, and  $t_{cf}$  is 2s and 2.8s, respectively.

Trajectories in Fig. 10(a) are corrected with different termination times. If it is decided that the vehicle should complete lane-changing ahead of schedule,  $t_{cf}$  is less than  $t_f$ , otherwise, it is larger than  $t_f$ . Fig. 10(a) indicates that the corrected trajectories have smooth and continued lateral accelerations, which are all limited under the threshold (0.4g). So the results in Fig. 10 are reasonable.

### C. TRAJECTORY REENTRY

Lastly, if it is infeasible to complete the lane-changing, the vehicle can return to its original lane, as shown in Fig. 2(c). The termination time for reentry is decided in (22). Considering that the returned trajectory has six equality constraints at the start point and the termination point, the six-order polynomial is appropriate for re-planning under these six hard constraints, which is expressed in (43).

$$Y_r(t) = \sum_{i=1}^6 (a_{ri} \cdot t^i), \quad t \in [t_r, t_{rf}] \quad (43)$$

where  $Y_r(t)$  represents the lateral displacement in the returning process,  $a_{r0}, \dots, a_{r6}$  are coefficients, which are obtained by

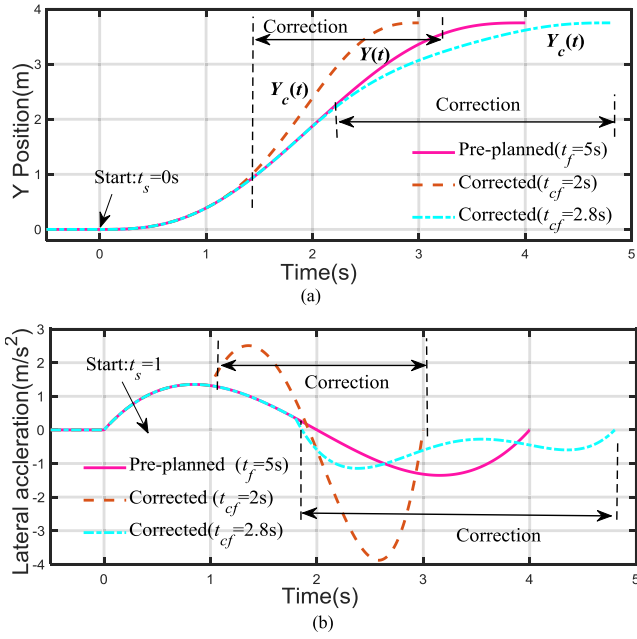


**FIGURE 10.** Comparisons between the pre-planned trajectory and corrected trajectories: (a). Trajectories. (b). Lateral accelerations.

solving the following problem:

$$J = \min \left\{ w_1 \cdot \frac{t_{rf} - t_r}{\hat{a}_y^2} \cdot \left( \int_{t_r}^{t_{rf}} \ddot{Y}_r(t) dt \right) + w_2 \cdot D[\ddot{Y}_r(t)] \right\}, \quad (44)$$

s.t.

$$\begin{cases} Y_r(t_r) = Y(t_r), \dot{Y}_r(t_r) = \dot{Y}(t_r), \ddot{Y}_r(t_r) = \ddot{Y}(t_r), \\ Y_r(t_{rf}) = 0, \dot{Y}_r(t_{rf}) = 0, \ddot{Y}_r(t_{rf}) = 0, \\ |Y(t)| \leq Y_{\max}, \\ |\dot{Y}_r(t)| \leq a_y \max, \\ |Y_r(t)| \leq j_y \max, \end{cases}$$

with

$$D[\ddot{Y}_r(t)] = \frac{\int_{t_r}^{t_{rf}} (\ddot{Y}_r(t))^2 dt - 2E[\ddot{Y}_r(t)] \cdot \int_{t_r}^{t_{rf}} \ddot{Y}_r(t) dt + E[\ddot{Y}_r(t)]^2}{t_{rf} - t_r},$$

$$E[\ddot{Y}_r(t)] = \frac{\int_{t_r}^{t_{rf}} \ddot{Y}_r(t) dt}{t_{rf} - t_r},$$

where the first target in (44) is to minimize the risk of sideslip, the second target is to minimize the fluctuation of lateral motion. The objective of (44) is more complex than (34) and (42) because the vehicle has enough time to return without sacrificing comfort.  $\hat{a}_y$  is the standard lateral acceleration,  $Y_{\max}$  is the max lateral displacement in the returning process,  $a_y \max$  is the threshold of lateral acceleration,  $C_{y\max}$  is the threshold of lateral jerk. (44) can be solved by *fmincon* function in MATLAB. Comparisons of the pre-planned trajectory

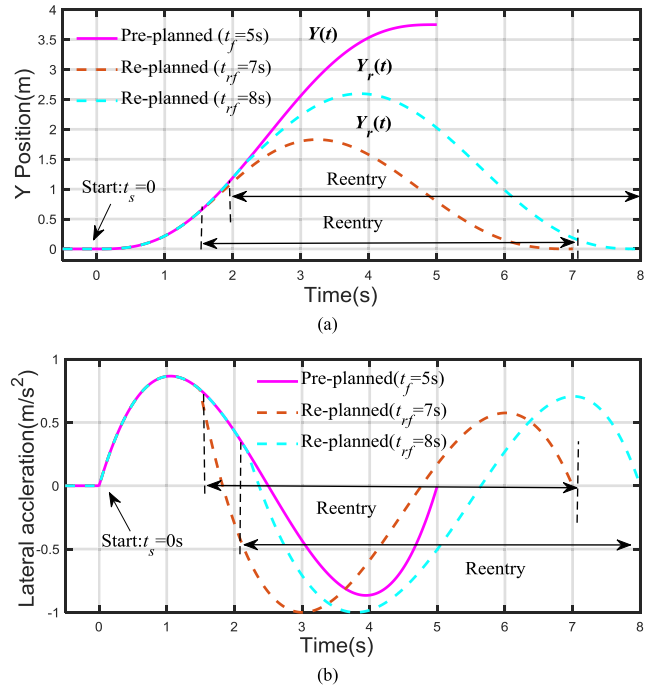


**FIGURE 11.** Comparisons between the pre-planned trajectory and returned trajectories: (a). Trajectories. (b). Lateral accelerations.

and the returned trajectories, as well as lateral accelerations are given in Fig. 11.

Fig. 11 indicates that the re-planned trajectories can smoothly transit from vehicle's current positions to the original lane with lateral accelerations limited in the allowable range, which reflects that the reentry can be completed steadily.

## V. STEERING STABILITY EVALUATION SYSTEM

Section III and section IV design the longitudinal motion planning model and the lateral motion planning model, respectively. In this section, a comprehensive evaluation system derived from vehicle dynamics is introduced to test the vehicle steering stability, including the stability of lane-changing and reentry.

Firstly, the lateral acceleration and longitudinal acceleration should be smooth, and the range of which should be limited to the friction circle [56], i.e.,

$$\sqrt{a_x^2 + a_y^2} \leq \mu \cdot g \quad (45)$$

where  $a_x$  is the vehicle longitudinal acceleration in the vehicle coordinate system, and  $a_y$  is vehicle lateral acceleration in the vehicle coordinate system.

Next, it needs to consider whether the longitudinal speed is in the resonable range. A speed profile is employed to provide an upper speed bound, any speed below this bound is allowable. Defining  $s(t)$  as the distance along the real path, the local minimum point of this longitudinal speed profile

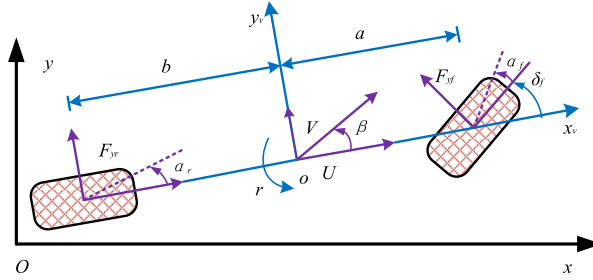


FIGURE 12. 2 DOF vehicle dynamic model.

is [57], [58]:

$$\min[U_x(s(t))] = \sqrt{\frac{\mu \cdot g}{\text{local max } |k|}}, \quad (46)$$

where  $U_x(s(t))$  denotes the longitudinal speed profile along the path,  $k$  is the path curvature:

$$k = \frac{\frac{\partial^2 y}{\partial x^2}}{\left(1 + \left(\frac{\partial y}{\partial x}\right)^2\right)^{3/2}}. \quad (47)$$

Extending from local minimum points to obtain a continued longitudinal speed profile, i.e.,

$$U_x(s(t+1)) = U_x(s(t)) + \sqrt{(\mu \cdot g)^2 - a_y(s(t))^2} \cdot |\Delta t|. \quad (48)$$

Finally, it needs to identify the vehicle handling stability when steering. The stable handing envelope that is derived from vehicle two degree-of-freedom (2DOF) dynamic model is adopted to construct the evaluation criteria [59].

The 2DOF model is seen in Fig. 12. In Fig. 12, the side slip angle and yaw rate of the vehicle have the following relationship:

$$\dot{\beta} = \frac{F_{yr} + F_{yf} \cdot \cos \delta_f}{m \cdot U} - r \approx \frac{F_{yr} + F_{yf}}{m \cdot U} - r, \quad (49)$$

where  $\beta$  is the side slip angle,  $F_{yr}$  and  $F_{yf}$  represent lateral force of the front axle and rear axle, respectively.  $\delta_f$  represents the front wheel angle,  $m$  is vehicle mass, and  $U$  is the longitudinal speed in the vehicle coordinate system, which is measured in real-time by the sensor. In (49), the vehicle is in a stable state when  $\dot{\beta}$  is approaching zero. So, the stable yaw rate is expressed as:

$$r_s = \frac{F_{yr} + F_{yf}}{m \cdot U}. \quad (50)$$

Neglecting the longitudinal tire force, the boundary of tire lateral force is related to the road friction coefficient:

$$|F_{yr} + F_{yf}| \leq m \cdot g \cdot \mu. \quad (51)$$

Therefore, the limitation of the stable yaw rate is:

$$|r_s| \leq \frac{g \cdot \mu}{\max(U)}. \quad (52)$$

Besides, the saturation of rear tires characteristic should also be considered. From the brush tire model for the rear tire,

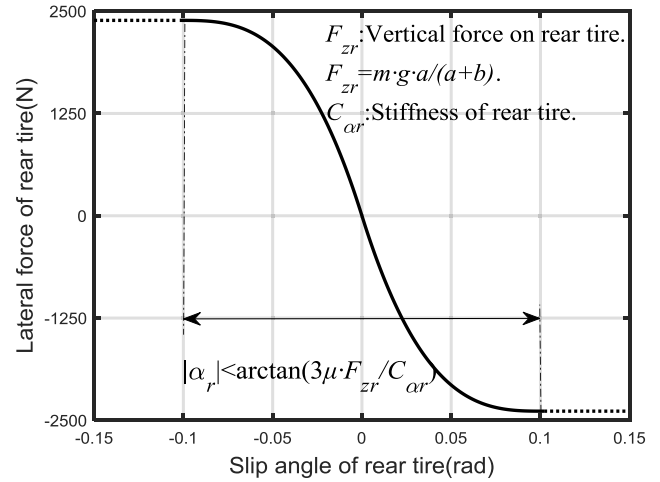


FIGURE 13. Brush tire model of rear tire.

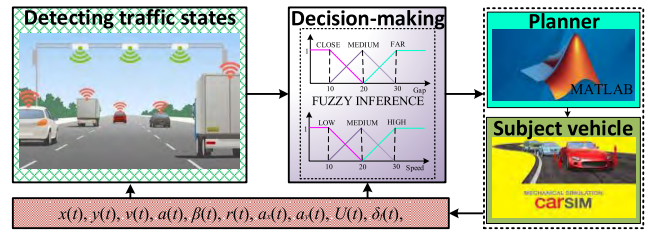


FIGURE 14. The simulation platform with MATLAB/CarSim.

the lateral force can be expressed by the tire slip angle, as depicted in Fig. 13 [60].

Fig. 13 presents that for rear tires, the peak  $\alpha$  that produces maximum lateral force is:

$$\alpha_r \leq \tan^{-1} \left( \frac{3m \cdot g \cdot \mu}{C_{ar}} \times \frac{a}{a+b} \right). \quad (53)$$

where  $a, b$  indicates the distance from the center of mass to the front and rear axles, respectively. The rear tire slip angle and the vehicle side slip angel have the following relationship under the small angle assumption:

$$\alpha_r \approx \beta - \frac{b \cdot r}{\max(U)}. \quad (54)$$

Introducing (53) into (54) to obtain the boundary of stable side slip angle:

$$|\beta_s| \leq \tan^{-1} \left( \frac{3m \cdot g \cdot \mu}{C_{ar}} \times \frac{a}{a+b} \right) + \frac{b \cdot r_s}{\max(U)}. \quad (55)$$

Combing (50) and (54), the stable handling envelope is built to identify the handling stability through the  $\beta$ - $r$  curve.

## VI. SIMULATIONS AND ANALYSES

In this section, the proposed approach will be tested by experiments with CarSim/MATLAB as the simulation platform, as seen in Fig. 14.

Fig. 14 presents a complete lane-changing process of the subject vehicle, including the detection of surrounding traffic states, the decision-making, the motion-planning, and

execution. The experiments in this section are designed to verify the motion planning model proposed above, while the detection technique and decision-making mechanism are not discussed. The studies of vehicle communication method and the decision-making model can refer to the works of Darbha *et al.* and Balal *et al.*, respectively [10], [61].

**TABLE 2. Parameters for simulation experiments and evaluations.**

Attribution	Parameter	Value
General motion-planning parameters	$\hat{D}$	$0.2m^2/s^4$
	$\hat{x}$	100m
	$\Delta\hat{v}_x$	2m/s
	$[w_1, w_2, w_3]$	[1,1,3]
	$t_p$	2.5s
	$\hat{d}$	2.5m
	$\varepsilon$	1
	$L_F(0)$	14m
	$L_R(0)$	11m
	$L_{Le}(0)$	0.2m
	$L_{La}(0)$	10m
	$v_{x0}$	70km/h
	$v_{xF}(0)$	60km/h
	$v_{xR}(0)$	55km/h
	$v_{xLe}(0)$	80km/h
	$v_{xLa}(0)$	73km/h
For simulation A (normal lane-changing)	$\mu$	0.85
	$l_{vF}, l_{vM}, l_{vLe}$	4.556
	$t_s$	0s
	$x_0$	0m
	$w$	3.75m
	$a_{xmax}$	$3m/s^2$
	$j_{xmax}$	$4m/s^3$
	$[a_{xF}(t), a_{xR}(t)]$	[0,0]
	$[a_{xLe}(t), a_{xLa}(t)]$	[0,0]
	$a_{cxmax}$	$3.5m/s^2$
For simulation B (trajectory correction)	$j_{cxmax}$	$4m/s^3$
	$t_c$	1.5s
	$[a_{xLe}(t), a_{xLa}(t)]$	$[-3m/s^2, 0]$
	$a_{rymax}$	$0.4m/s^2$
For simulation C (trajectory reentry)	$j_{rymax}$	$0.5m/s^3$
	$a_{ymax}$	0.4g
	$j_{ymax}$	$0.5g/s$
	$\hat{a}_y$	0.3g
	$m$	1270kg
Vehicle dynamics parameters	$a$	1015mm
	$b$	1895mm
	$C_{af}$	69959.2N/rad
	$C_{ar}$	38647.87N/rad

Simulation and evaluation parameters are in Table 2. In Table 2, the parameter  $\varepsilon$  affects the longitudinal planning results. In this paper, the parameter  $\varepsilon$  is determined based on the timeliness and optimization effects, please see APPENDIX for details. In addition, optimization algorithms used in the solution process are also summarized in APPENDIX. The following simulation experiments are conducted independently, with their respective prerequisite.

#### A. NORMAL LANE-CHANGING SCENARIO

**Prerequisite:** in the lane-changing period of the subject vehicle, surrounding vehicles are driving in the straight-line with constant speeds, as described in Fig. 2(a).

In Fig. 14, the planner plans a normal lane-changing trajectory for the subject vehicle at first. Based on parameters in Table 2, the termination time for lane-changing decided by the longitudinal model is 3.4 s ( $t_f$ ). Using  $t_f$  as the input, the lateral model provides an optimal reference trajectory from the start to the termination point. The total planning time is 0.099s with an i5 processor. The trajectories of vehicles in this scenario are given in Fig. 15. Note that vehicles in Fig. 15 appear in the same traffic scene at the same time. To make simulation results clearer, they are separated into Fig. 15(a) and Fig. 15(b).

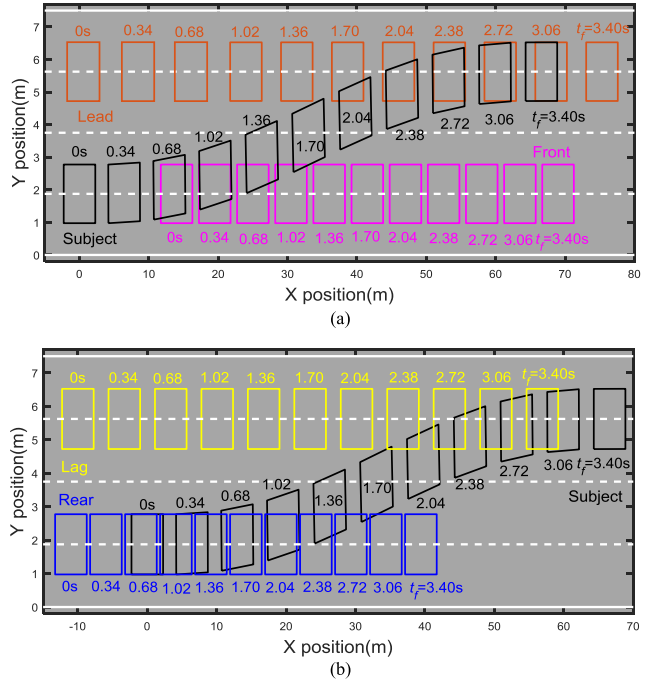


**FIGURE 15. Vehicle trajectories in the normal lane-changing scenario (by the proposed model): (a). Trajectories of the subject vehicle, front vehicle, and lead vehicle. (b). Trajectories of the subject vehicle, rear vehicle, and lag vehicle.**

It is seen in Fig. 15 that the subject vehicle does not collide with any surrounding vehicle throughout the lane-change process, therefore, in this experiment, the trajectory planned for the normal lane-changing scheme is collision-free. Fig. 15 presents a typical scene of overtaking and lane-changing, the APF algorithm is a classical method to deal with such problem [19]. So, it is employed as the competitor with the details seen in APPENDIX. On the premise of keeping the same simulation parameters as the proposed model, simulation results reveal that the subject vehicle with the reference trajectory planned by the conventional APF algorithm would collide with the lead vehicle, as shown in Fig. 16. In Fig. 16, the subject vehicle collides with the lead vehicle at 0.68s and 1.02s. Although APF can make the

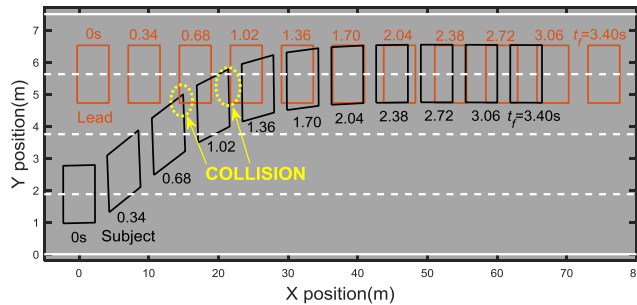


**FIGURE 16.** Trajectories of the subject vehicle and the lead vehicle in the normal lane-changing scenario (by conventional APF algorithm).

subject vehicle reach the target lane, when there are multiple obstacles, the planned trajectory may not be ideal, and collisions may arise. Next, the lane-changing performance of the subject vehicle in Fig. 15 is tested according to Section V, with results shown in Fig. 17.

Fig. 17(a)–(b) illustrate that both lateral and longitudinal accelerations are smooth, and are all limited in the friction circle. Fig. 17(c) shows that the longitudinal velocity is under the speed bound, and Fig. 17(d) presents that the  $\beta$ - $r$  curve is in the stable handling envelope. Comparisons and evaluations above confirm that the trajectory planned by the proposed model is collision-free and stable. This approach can deal with a conventional trajectory planning problem.

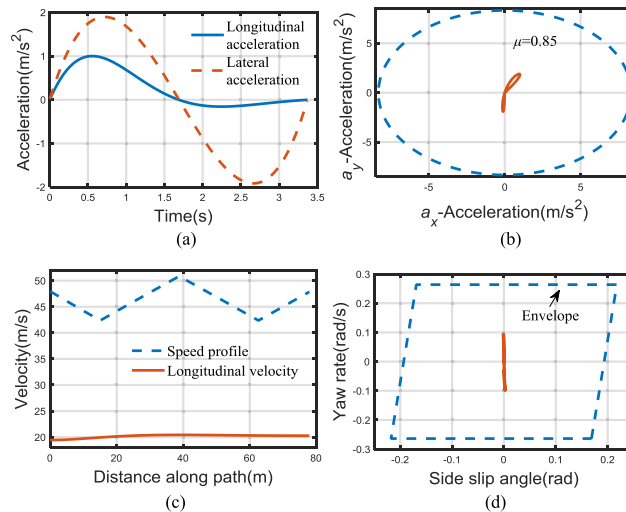


**FIGURE 17.** Stability evaluations of the vehicle in the normal lane-changing scenario: (a) Longitudinal and lateral accelerations. (b) Friction circle. (c) Longitudinal speed profile. (d) Stable handling envelope.

## B. TRAJECTORY CORRECTION SCENARIO

**Prerequisite:** in the normal lane-changing process of the subject vehicle, the lead vehicle decelerates at time  $t_c$ , as depicted in Fig. 2 (b).

According to this prerequisite and parameters in Table 2, the decision-making module judges that the pre-planned

trajectory is not safe, then the planner corrects the reference trajectory. Using parameters in Table 2, the longitudinal model updates the termination time to 3s( $t_{cf}$ ), solutions are obtained within 0.12s by an i5processor, and simulation results are shown in Fig. 18.

Fig. 18 presents that the proposed planning strategy is valid because the subject vehicle does not collide with any surrounding vehicle during the correcting period. Next, the conventional quartic polynomial model in Table 1 is employed for the comparison, with the details in APPENDIX. For this conventional planner, simulation parameters also come from Table 2. One of the representative simulation results is shown in Fig. 19.

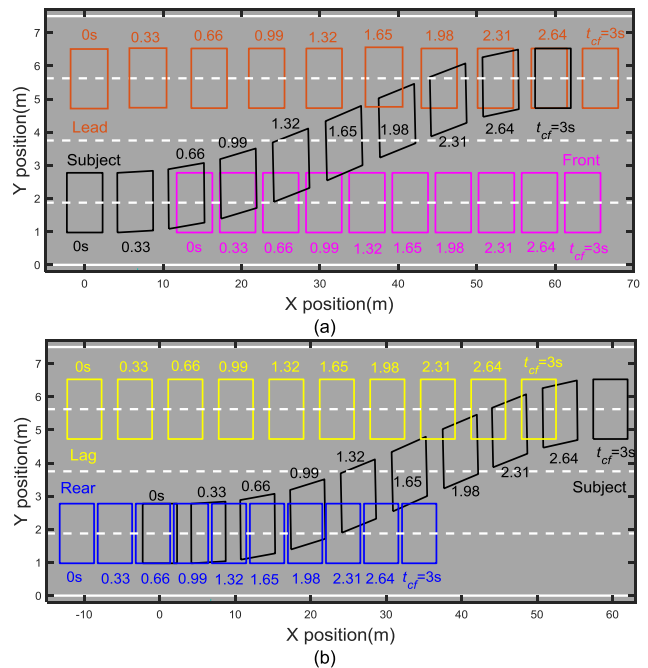


**FIGURE 18.** Vehicle trajectories in the correction scenario (by the proposed model): (a) Trajectories of the subject vehicle, front vehicle, and lead vehicle. (b) Trajectories of the subject vehicle, rear vehicle, and lag vehicle.

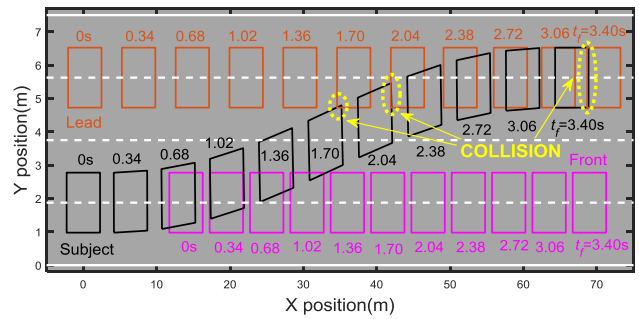


**FIGURE 19.** Trajectories of the subject vehicle and the lead vehicle in experiment B (by the conventional technique).

Fig. 19 shows that the subject vehicle collides with the lead vehicle at 1.7s, 2.04s, and 3.40s if it travels along

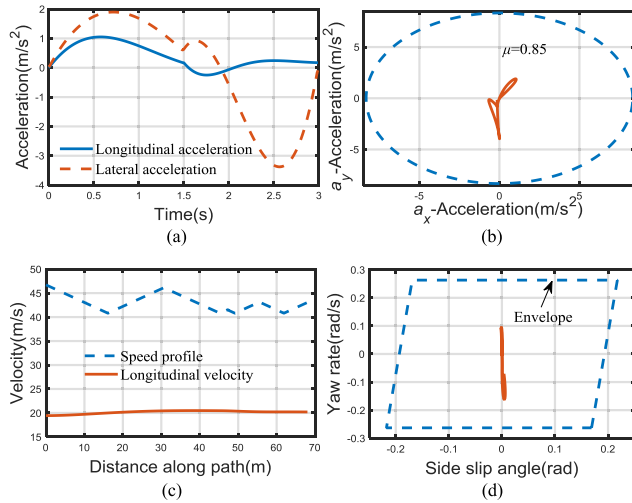


**FIGURE 20.** Stability evaluations of the subject vehicle in correction scenario: (a). Longitudinal and lateral accelerations. (b). Friction circle. (c). Longitudinal speed profile. (d). Stable handling envelope.

the reference trajectory planned by the quintic polynomial. In fact, for conventional techniques without trajectory re-planning capacity, collisions are unavoidable because the termination point is fixed. The quintic polynomial is one of the examples, a similar result in Fig. 19 would appear by other planners in Table 1. In Fig. 18, the stability of the subject vehicle is evaluated, with results given in Fig. 20.

Using the same analysis method as Fig. 17 to evaluate results in Fig. 20, it can conclude that the subject vehicle is stable when it travels along the corrected trajectory to accomplish lane-changing. Comparisons and evaluations above indicate that the trajectory corrected is feasible.

### C. TRAJECTORY REENTRY SCENARIO

**Prerequisite:** in the normal lane-changing process, there is no vehicle on lane 2, so the separated vehicle cuts into lane 2 at time  $t_{rf}$ , the reference trajectory of the separated vehicle cannot be predicted by the subject vehicle, as in Fig. 2(c).

Based on this prerequisite, the decision-making module commands the subject vehicle to return to the target lane as it may collide with the separated vehicle.

According to simulation parameters in Table 2, the longitudinal model decides the new termination time ( $t_{rf}$ ) as 8s. The trajectory is re-planned within 0.18s when using an i5 processor, and the simulation results of this experiment are presented in Fig. 21. Furthermore, taking the same conventional planner as the last simulation experiment for comparison, one of the representative simulation results is shown in Fig. 22.

Fig. 21 reflects that the subject vehicle does not collide with any surrounding vehicle in the reentry process.

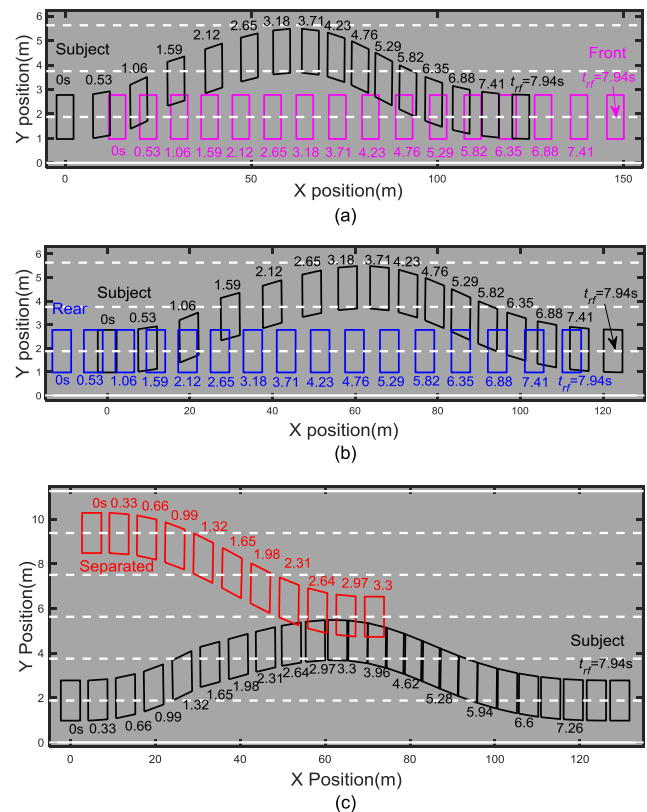


**FIGURE 21.** Vehicle trajectories in reentry scenario (by the proposed model): (a). Trajectories of the subject vehicle and front vehicle. (b). Trajectories of the subject vehicle and rear vehicle. (c) Trajectories of the subject vehicle and separated vehicle.

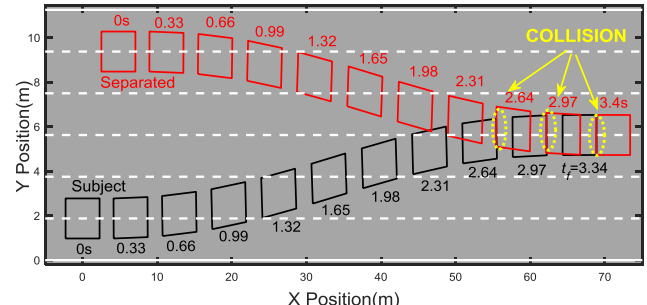


**FIGURE 22.** Trajectories of the subject vehicle and the lead vehicle in the experiment C (by the conventional technique).

However, for the conventional method, simulation result in Fig. 22 reveals that the subject vehicle would collide with the separated vehicle at 2.64 s, 2.97 s, and 3.40 s. Moreover, evaluation results of the steering stability of the subject vehicle in Fig. 21 are addressed in Fig. 23.

The subject vehicle is stable when it travels along the re-planned trajectory to return because the motion characteristics shown in Fig. 23 all meet stability criterions proposed in section V. Comparisons and evaluations above prove that proposed research is effective to handle emergencies in the normal lane-changing process.

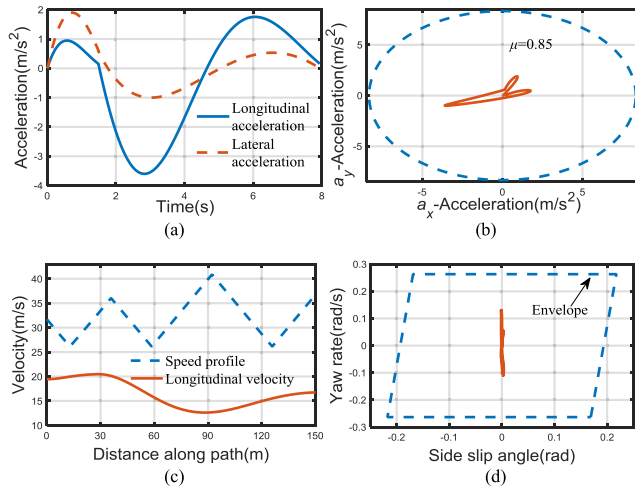


**FIGURE 23.** Stability evaluations of the subject vehicle in reentry scenario: (a). Longitudinal and lateral accelerations. (b). Friction circle. (c). Longitudinal speed profile. (d). Stable handling envelope.

## VII. CONCLUSION

In this paper, a lane-changing motion planning model that consists of the longitudinal planning model and the lateral planning model is designed for intelligent vehicles in dynamical traffic environments. The most significant advantage of this research is that the model can plan a smooth and continued reference trajectory from the vehicle's current position to varying destinations. This endues the planner with the trajectory re-planning ability in the vehicle lane-changing process, which is of great importance to prevent potential collisions caused by variations of traffic states. Complex iterations are avoided in optimization to improve the timeliness. Advantages of this approach are proved by comparisons with conventional techniques. Future works will concentrate on the decision-making module and the execution module to build up a complete system.

## APPENDIX A THE QUINTIC POLYNOMIAL MODEL

The quintic polynomial used in this paper is to plan the vehicle lateral lane-changing trajectory, the longitudinal trajectories are planned by difference models, i.e.,

1) In Fig. 4 and Fig. 8, longitudinal trajectories are planned with constant longitudinal speed, that is:

$$x(t) = x_0 + v_x \cdot t, \quad (\text{A.1})$$

where  $x_0$  is the initial longitudinal position,  $v_x$  is the longitudinal velocity.

2).The longitudinal trajectories in Fig. 19 and Fig. 22 are planned according to the model proposed in (1)-(12), as it has only three parameters, this is convenient for planning.

Using the quintic polynomial, the lateral lane-changing trajectory is planned as follows:

$$y(t) = a_0 + a_1 \cdot t + a_2 \cdot t^2 + a_3 \cdot t^3 + a_4 \cdot t^4 + a_5 \cdot t^5, \quad (\text{A.2})$$

where  $y(t)$  represents the lateral displacement,  $a_0, \dots, a_5$  are coefficients. Constraints on lateral motions are expressed as:

$$y(0) = 0, \quad y(t_f) = w, \quad (\text{A.3a})$$

$$\dot{y}(0) = 0, \quad \dot{y}(t_f) = 0, \quad (\text{A.3b})$$

$$\ddot{y}(0) = 0, \quad \ddot{y}(t_f) = 0, \quad (\text{A.3c})$$

where  $t_f$  is the termination time of lane-changing, and  $w$  is the lane-width, (A.3a) is to satisfy location constraints of vehicles at the start and end points. (A.3b) and (A.3c) ensure the vehicle has a smooth and continued lateral velocity and lateral acceleration, respectively. (A.2) has six hard constraints, and the quintic polynomial has six coefficients, so these coefficients can be solved directly from the following equation when giving  $t_f$  in (17):

$$\begin{bmatrix} 1 & 0 & 0 & 0 & 0 & 0 \\ 1 & t_f & t_f^2 & t_f^3 & t_f^4 & t_f^5 \\ 0 & 1 & 0 & 0 & 0 & 0 \\ 0 & 1 & 2t_f & 3t_f^2 & 4t_f^3 & 5t_f^4 \\ 0 & 0 & 2 & 0 & 0 & 0 \\ 0 & 0 & 2 & 6t_f & 12t_f^2 & 20t_f^3 \end{bmatrix} \begin{bmatrix} a_0 \\ a_1 \\ a_2 \\ a_3 \\ a_4 \\ a_5 \end{bmatrix} = \begin{bmatrix} 0 \\ w \\ 0 \\ 0 \\ 0 \\ 0 \end{bmatrix}. \quad (\text{A.4})$$

## APPENDIX B THE APF ALGORITHM

The model of the APF is shown in Fig. A1. In Fig. A1, the repulsive field is produced by the front vehicle, and the gravitational field is produced by the target position. The longitudinal distance between the target position and the obstacle is  $d_{TV}$ . The repulsive force field is an elliptic region with a long axis of  $l_1$ , and a short axis of  $l_2$ . And the gravitational field is a circular region, with the radius of  $R$ . The repulsive force on the subject vehicle is:

$$\vec{F}_r = \begin{cases} \sigma_1 \cdot \left( \frac{1}{\rho_{FS}} - \frac{1}{\rho_F} \right) \cdot \vec{a}_{FS}, & 0 < \rho_F < \rho_{FS} \\ 0, & \rho_F \geq \rho_{FS} \end{cases}, \quad (\text{A.5})$$

where  $\vec{F}_r$  is the repulsive force,  $\sigma_1$  is the gain coefficient.  $\rho_{FS}$  represents the distance between the subject vehicle and the obstacle.  $\rho_F$  represents the effective range of the obstacle,  $\vec{a}_{FS}$  is a unit vector from the obstacle to the subject vehicle.

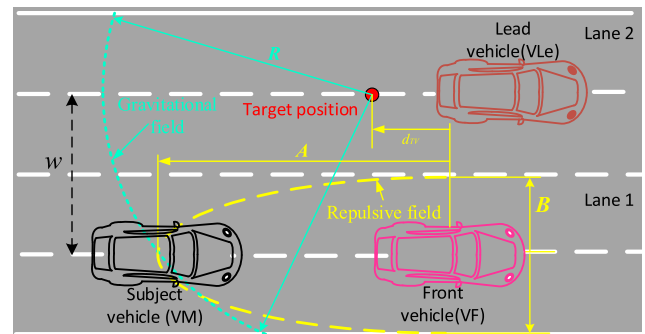


**FIGURE A1.** Model of APF.

The attractive force on the subject vehicle is:

$$\vec{F}_a = \sigma_2 \cdot \rho_{ST} \cdot \vec{a}_{ST}, \quad (\text{A.6})$$

where  $\vec{F}_a$  denotes the attractive force,  $\sigma_2$  is the gain coefficient.  $\rho_{ST}$  is the effective range of the target,  $\vec{a}_{ST}$  is the unit vector from the subject vehicle to its target. At time  $t$ , the resultant force of the repulsive force and attractive force decides the motion direction of the subject vehicle, so the yaw angle is determined, which is calculated as:

$$\varphi(t) = \frac{|\vec{F}_r| \cdot (\theta_{FS} + \theta_{ST})}{\sqrt{|\vec{F}_r|^2 + |\vec{F}_a|^2 - 2|\vec{F}_r| \cdot |\vec{F}_a| \cdot \cos(\theta_{FS} + \theta_{ST})}}, \quad (\text{A.7})$$

$$\theta_{ST} = \arccos \frac{|x(t) - x_T(t)|}{\sqrt{(x(t) - x_T(t))^2 + (y(t) - y_T(t))^2}}, \quad (\text{A.8})$$

$$\theta_{FS} = \arccos \frac{|x_F(t) - x(t)|}{\sqrt{(x_F(t) - x(t))^2 + (y_F(t) - y(t))^2}}, \quad (\text{A.9})$$

where  $(x(t), y(t))$ ,  $(x_F(t), y_F(t))$ , and  $(x_T(t), y_T(t))$  denote position coordinate of the subject vehicle, the obstacle, and the target position in geodetic coordinates, respectively.  $(x_F(t), y_F(t))$  is taken as zero when the subject vehicle is out of the repulsive field. The trajectory is planned by integrating along the yaw angle.

## APPENDIX C

### DECIDING THE PARAMETER $\varepsilon$ IN IPF ALGORITHM

It has been mentioned in (11) that the parameter  $\varepsilon$  has a great impact on the performance of the IPF algorithm, then the longitudinal planning results are affected

Generally, optimization results would be closer to the global optimal solution when the parameter  $\varepsilon$  becomes smaller. For simulation parameters in Table 2, optimization results of the longitudinal motion that vary with  $\varepsilon$  are expressed in Table A.1. According to Table A.1, the time consumption of optimization that varies with the specific value of  $\varepsilon$  of the IPF algorithm is presented in Fig. A2.

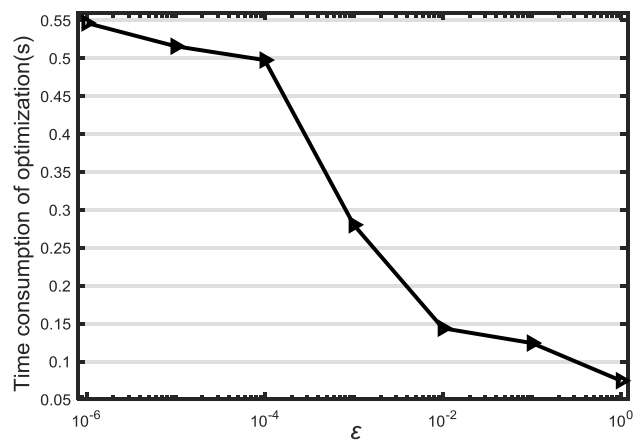


FIGURE A2. Time consumption of optimization varies with  $\varepsilon$ .

In Table A.1, the result of longitudinal planning does not change significantly with the parameter  $\varepsilon$ , and the iteration stops when  $\varepsilon$  is less than  $1 \times 10^{-6}$ , this reflects that the solution is the closest to the global optimal result when  $\varepsilon$  is

TABLE A.1. Longitudinal optimization result varies with  $\varepsilon$ .

$\varepsilon$	A	B	C
1	1.0112	3.3736	2.1359
$1 \times 10^{-1}$	1.0074	3.3748	2.1436
$1 \times 10^{-2}$	1.0060	3.3758	2.1486
$1 \times 10^{-3}$	1.0610	3.3759	2.1492
$1 \times 10^{-4}$	1.0106	3.3772	2.1500
$1 \times 10^{-5}$	1.0106	3.3772	2.1500
$1 \times 10^{-6}$	1.0106	3.3772	2.1500
$1 \times 10^{-7}$	Iteration stopped	Iteration stopped	Iteration stopped

TABLE A.2. Optimization algorithms used in this paper.

Optimization problem	Optimization algorithm
Problem (6)	IPF algorithm
Problem (16)	IPF algorithm
Problem (21)	IPF algorithm
Problem (32)	'active-set' algorithm in fmincon
Problem (34)	'sqp' algorithm in fmincon
Problem (42)	'sqp' algorithm in fmincon
Problem (44)	Default algorithm in fmincon

$1 \times 10^{-6}$  in the IPF algorithm. Conversely, Fig. A2 shows that the timeliness of the IPF algorithm varies significantly with  $\varepsilon$ . As a result,  $\varepsilon$  is finally decided as 1 when considering the real-time performance of the planner. When  $\varepsilon$  is 1, there is little difference between the solution and the global optimal result within the scope of iteration, while the timeliness of optimization is greatly improved.

## APPENDIX D OPTIMIZATION ALGORITHMS FOR SOLUTION

Many optimizations are involved in the planning process with the proposed model. The relevant optimization algorithms are summarized in Table A.2.

## REFERENCES

- [1] D. Zhao et al., "Accelerated evaluation of automated vehicles safety in lane-change scenarios based on importance sampling techniques," *IEEE Trans. Intell. Transp. Syst.*, vol. 18, no. 3, pp. 595–607, Mar. 2017.
- [2] J. Kim, J. Kim, G.-J. Jang, and M. Lee, "Fast learning method for convolutional neural networks using extreme learning machine and its application to lane detection," *Neural Netw.*, vol. 87, pp. 109–121, Mar. 2017.
- [3] K. Yang, S. I. Guler, and M. Menendez, "Isolated intersection control for various levels of vehicle technology: Conventional, connected, and automated vehicles," *Transp. Res. C, Emerg. Techn.*, vol. 72, pp. 109–129, Nov. 2016.
- [4] Z. Wang, W. Deng, S. Zhang, and J. Shi, "Vehicle automatic lane changing based on model predictive control," *SAE Int. J. Passenger Cars-Electron. Electr. Syst.*, vol. 9, no. 1, pp. 231–236, May 2016.
- [5] K. Han, E. Lee, M. Choi, and S. B. Choi, "Adaptive scheme for the real-time estimation of tire-road friction coefficient and vehicle velocity," *IEEE-ASME Trans. Mechatronics*, vol. 22, no. 4, pp. 1508–1518, Aug. 2017.
- [6] A. B. Hillel, R. Lerner, D. Levi, and G. Raz, "Recent progress in road and lane detection: A survey," *Mach. Vis. Appl.*, vol. 25, no. 3, pp. 727–745, 2014.
- [7] J. Wang, J. Wang, R. Wang, and C. Hu, "A framework of vehicle trajectory replanning in lane exchanging with considerations of driver characteristics," *IEEE Trans. Veh. Technol.*, vol. 66, no. 5, pp. 3583–3596, May 2017.
- [8] J. Nie, J. Zhang, W. Ding, X. Wan, X. Chen, and B. Ran, "Decentralized cooperative lane-changing decision-making for connected autonomous vehicles," *IEEE Access*, vol. 4, pp. 9413–9420, 2016.

- [9] Y. Hou, P. Edara, and C. Sun, "Situation assessment and decision making for lane change assistance using ensemble learning methods," *Expert Syst. Appl.*, vol. 42, no. 8, pp. 3875–3882, May 2015.
- [10] E. Balal, R. L. Cheu, and T. Sarkodie-Gyan, "A binary decision model for discretionary lane changing move based on fuzzy inference system," *Transp. Res. C, Emerg. Technol.*, vol. 67, pp. 47–61, Jun. 2016.
- [11] X. Li, Z. Sun, D. Cao, Z. He, and Q. Zhu, "Real-time trajectory planning for autonomous urban driving: Framework, algorithms, and verifications," *IEEE/ASME Trans. Mechatronics*, vol. 21, no. 2, pp. 740–753, Apr. 2016.
- [12] G. Cesari, G. Schildbach, A. Carvalho, and F. Borrelli, "Scenario model predictive control for lane change assistance and autonomous driving on highways," *IEEE Intell. Transp. Syst. Mag.*, vol. 9, no. 3, pp. 23–35, Jul. 2017.
- [13] M. Maurer, J. C. Gerdes, B. Lenz, and H. Winner, *Autonomous Driving: Technical, Legal and Social Aspects*. Berlin, Germany: Springer-Verlag, 2016.
- [14] S. Han, B. Choi, and J. Lee, "A precise curved motion planning for a differential driving mobile robot," *Mechatronics*, vol. 18, no. 9, pp. 484–486, Nov. 2008.
- [15] D. González, J. Pérez, V. Milanés, and F. Nashashibi, "A review of motion planning techniques for automated vehicles," *IEEE Trans. Intell. Transp. Syst.*, vol. 17, no. 4, pp. 1135–1145, Apr. 2016.
- [16] I. Yang, H. J. Kim, W. H. Jeon, and H. Kim, "Development of realistic shortest path algorithm considering lane changes," *J. Adv. Transp.*, vol. 50, no. 4, pp. 541–551, Jun. 2016.
- [17] D. Madås et al., "On path planning methods for automotive collision avoidance," in *Proc. IEEE Intell. Vehicles Symp. (IV)*, Gold Coast, QLD, Australia, Jul. 2013, pp. 931–937.
- [18] X. Lan and S. Di Cairano, "Continuous curvature path planning for semi-autonomous vehicle maneuvers using RRT," in *Proc. Eur. Control Conf. (ECC)*, Linz, Austria, vol. 2015, pp. 2360–2365.
- [19] C. Katrakazas, M. Quddus, W.-H. Chen, and L. Deka, "Real-time motion planning methods for autonomous on-road driving: State-of-the-art and future research directions," *Transp. Res. C, Emerg. Technol.*, vol. 60, pp. 416–442, Nov. 2015.
- [20] S. B. Mehdi, R. Choe, and N. Hovakimyan, "Avoiding multiple collisions through trajectory replanning using piecewise Bézier curves," in *Proc. 54th IEEE Conf. Decis. Control (CDC)*, Osaka, Japan, Dec. 2015, pp. 2755–2760.
- [21] B. Zhu, J. Zhao, S. Yan, and W. Den, "Personalized lane-change assistance system with driver behavior identification," *IEEE Trans. Veh. Technol.*, vol. 67, no. 11, pp. 10293–10306, Nov. 2018.
- [22] S. Schnelle, J. Wang, H. Su, and R. Jagacinski, "A driver steering model with personalized desired path generation," *IEEE Trans. Syst., Man, Cybern., Syst.*, vol. 47, no. 1, pp. 111–120, Jan. 2017.
- [23] J. Suh, H. Chae, and K. Yi, "Stochastic model-predictive control for lane change decision of automated driving vehicles," *IEEE Trans. Veh. Technol.*, vol. 67, no. 6, pp. 4771–4782, Jun. 2018.
- [24] S. Schnelle, J. Wang, H.-J. Su, and R. Jagacinski, "A personalizable driver steering model capable of predicting driver behaviors in vehicle collision avoidance maneuvers," *IEEE Trans. Human-Mach. Syst.*, vol. 47, no. 5, pp. 625–635, Oct. 2017.
- [25] L. Wan, P. Raksincharoensak, and M. Nagai, "Study on automatic driving system for highway lane change maneuver using driving simulator," *J. Mech. Syst. Transp. Logistics*, vol. 4, no. 2, pp. 65–78, 2011.
- [26] J. Funke and J. C. Gerdes, "Simple clothoid lane change trajectories for automated vehicles incorporating friction constraints," *J. Dyn. Syst., Meas., Control*, vol. 138, no. 2, Feb. 2016, Art. no. 021002.
- [27] D. Soudbaksh, A. Eskandarian, and D. Chichka, "Vehicle collision avoidance maneuvers with limited lateral acceleration using optimal trajectory control," *J. Dyn. Syst., Meas., Control*, vol. 135, no. 4, Jul. 2013, Art. no. 041006.
- [28] Q. H. Do, H. Tehrani, S. Mita, M. Egawa, K. Muto, and K. Yoneda, "Human drivers based active-passive model for automated lane change," *IEEE Intell. Transp. Syst. Mag.*, vol. 9, no. 1, pp. 42–56, Jan. 2017.
- [29] F. You, R. Zhang, G. Lie, H. Wang, H. Wen, and J. Xu, "Trajectory planning and tracking control for autonomous lane change maneuver based on the cooperative vehicle infrastructure system," *Expert Syst. Appl.*, vol. 42, no. 14, pp. 5932–5946, 2015.
- [30] H. Bai, J. Shen, L. Wei, and Z. Feng, "Accelerated lane-changing trajectory planning of automated vehicles with vehicle-to-vehicle collaboration," *J. Adv. Transp.*, vol. 2017, Jul. 2017, Art. no. 8132769.
- [31] S. Schnelle, J. Wang, R. Jagacinski, and H.-J. Su, "A feedforward and feedback integrated lateral and longitudinal driver model for personalized advanced driver assistance systems," *Mechatronics*, vol. 50, pp. 177–188, Apr. 2018.
- [32] M. F. M. Ghani, J. M. Taib, and A. Dzakaria, "Feasibility study on the implementation of cubic motion curve for vehicle trajectory planning," *Adv. Mech. Eng.*, vol. 7, no. 1, pp. 1–12, Jan. 2015.
- [33] R. Huang, H. Liang, P. Zhao, B. Yu, and X. Geng, "Intent-estimation-and motion-model-based collision avoidance method for autonomous vehicles in urban environments," *Appl. Sci.*, vol. 7, no. 5, p. 457, May 2017.
- [34] G. Zhuo, C. Wu, and F. Zhang, "Model predictive control for feasible region of active collision avoidance," SAE, Pennsylvania, PA, USA, Tech. Paper 2017-01-0045, Mar. 2017.
- [35] R. Kala and K. Warwick, "Multi-level planning for semi-autonomous vehicles in traffic scenarios based on separation maximization," *J. Intell. Robot. Syst.*, vol. 72, nos. 3–4, pp. 559–590, Dec. 2013.
- [36] T. Shamir, "How should an autonomous vehicle overtake a slower moving vehicle: Design and analysis of an optimal trajectory," *IEEE Trans. Autom. Control*, vol. 49, no. 4, pp. 607–610, Apr. 2004.
- [37] S. Glaser, B. Vanholme, S. Mammar, D. Gruyer, L. Nouveliere, "Maneuver-based trajectory planning for highly autonomous vehicles on real road with traffic and driver interaction," *IEEE Trans. Intell. Transp. Syst.*, vol. 11, no. 3, pp. 589–606, Sep. 2010.
- [38] W. Lim, S. Lee, M. Sunwoo, and K. Jo, "Hierarchical trajectory planning of an autonomous car based on the integration of a sampling and an optimization method," *IEEE Trans. Intell. Transp. Syst.*, vol. 19, no. 2, pp. 613–626, Feb. 2018.
- [39] J. Nilsson, M. Bränström, E. Coelingh, and J. Fredriksson, "Lane change maneuvers for automated vehicles," *IEEE Trans. Intell. Transp. Syst.*, vol. 18, no. 5, pp. 1087–1096, May 2017.
- [40] B. Li, Y. Zhang, Y. Feng, Y. Zhang, Y. Ge, and Z. Shao, "Balancing computation speed and quality: A decentralized motion planning method for cooperative lane changes of connected and automated vehicles," *IEEE Trans. Intell. Veh.*, vol. 3, no. 3, pp. 340–350, Sep. 2018.
- [41] S. Moon, U. Lee, and D. H. Shim, "Study on real-time obstacle avoidance for unmanned ground vehicles," in *Proc. ICCAS*, Gyeonggi-do, South Korea, Oct. 2013, pp. 1332–1335.
- [42] W. Wang, J. Xi, C. Liu, and X. Li, "Human-centered feed-forward control of a vehicle steering system based on a driver's path-following characteristics," *IEEE Trans. Intell. Transp. Syst.*, vol. 18, no. 6, pp. 1440–1453, Jun. 2017.
- [43] M. T. Wolf and J. W. Burdick, "Artificial potential functions for highway driving with collision avoidance," in *Proc. IEEE Int. Conf. Robot. Automat.*, Pasadena, CA, USA, May 2008, pp. 3731–3736.
- [44] J. Ji, A. Khajepour, W. W. Melek, and Y. Huang, "Path planning and tracking for vehicle collision avoidance based on model predictive control with multiconstraints," *IEEE Trans. Ultrason. Eng.*, vol. 66, no. 2, pp. 952–964, Feb. 2017.
- [45] B. Zhou, Y. Wang, G. Yu, and X. Wu, "A lane-change trajectory model from drivers' vision view," *Transp. Res. C, Emerg. Technol.*, vol. 85, pp. 609–627, Dec. 2017.
- [46] G. Xu, L. Liu, Y. Ou, and Z. Song, "Dynamic modeling of Driver control strategy of lane-change behavior and trajectory planning for collision prediction," *IEEE Trans. Intell. Transp. Syst.*, vol. 13, no. 3, pp. 1138–1155, Sep. 2012.
- [47] G. Geng, Z. Wu, H. Jiang, L. Sun, and C. Duan, "Study on path planning method for imitating the lane-changing operation of excellent drivers," *Appl. Sci.*, vol. 8, no. 5, p. 814, May 2018.
- [48] S. Dixit et al., "Trajectory planning and tracking for autonomous overtaking: State-of-the-art and future prospects," *Annu. Rev. Control*, vol. 45, pp. 76–86, Mar. 2018.
- [49] Z. Gao, W. Yan, and H. Li, "Design of the time-gap-dependent robust headway control algorithm for ACC vehicles," *Int. J. Veh. Des.*, vol. 70, no. 4, pp. 325–340, 2016.
- [50] R. Dang, J. Wang, S. E. Li, and K. Li, "Coordinated adaptive cruise control system with lane-change assistance," *IEEE Trans. Intell. Transp. Syst.*, vol. 16, no. 5, pp. 2373–2383, Oct. 2015.
- [51] H. Park, C. Oh, J. Moon, and S. Kim, "Development of a lane change risk index using vehicle trajectory data," *Accident Anal. Prevention*, vol. 110, pp. 1–8, Jan. 2018.
- [52] Y. Luo, Y. Xiang, K. Cao, and K. Li, "A dynamic automated lane change maneuver based on vehicle-to-vehicle communication," *Transp. Res. C, Emerg. Technol.*, vol. 62, pp. 87–102, Jan. 2016.

- [53] J. F. Bonnans, J. C. Gilbert, C. Lemaréchal, and C. A. Sagastizábal, *Numerical Optimization*. Berlin, Germany: Springer-Verlag, 2003, pp. 353–456.
- [54] D. Halpern, H. B. Wilson, and L. H. Turcotte, *Advanced Mathematics and Mechanics Applications Using MATLAB*, 3rd ed. Denver, CO, USA: CRC Press, 2003, pp. 567–609.
- [55] D. Y. Xue and Y. Q. Chen, *Solving Applied Mathematical Problems with MATLAB*. Denver, CO, USA: CRC Press, 2009, pp. 45–59.
- [56] Y. Chen, H. Peng, and J. W. Grizzle, “Fast trajectory planning and robust trajectory tracking for pedestrian avoidance,” *IEEE Access*, vol. 5, pp. 9304–9317, 2017.
- [57] N. R. Kapania, J. Subosits, and J. C. Gerdes, “A sequential two-step algorithm for fast generation of vehicle racing trajectories,” *J. Dyn. Syst., Meas., Control*, vol. 138, no. 9, Sep. 2016, pp. 1–12.
- [58] K. Kritayakirana and J. C. Gerdes, “Autonomous vehicle control at the limits of handling,” *Int. J. Veh. Auton. Syst.*, vol. 10, no. 4, pp. 271–296, Jun. 2012.
- [59] C. E. Beal and J. C. Gerdes, “Model predictive control for vehicle stabilization at the limits of handling,” *IEEE Trans. Control Syst. Technol.*, vol. 21, no. 4, pp. 1258–1269, Jul. 2013.
- [60] S. M. Erlien, S. Fujita, and J. C. Gerdes, “Shared steering control using safe envelopes for obstacle avoidance and vehicle stability,” *IEEE Trans. Intell. Transp. Syst.*, vol. 17, no. 2, pp. 441–451, Feb. 2016.
- [61] S. Darbha, S. Konduri, and P. R. Pagilla, “Benefits of V2V communication for autonomous and connected vehicles,” *IEEE Trans. Intell. Transp. Syst.*, to be published. doi: [10.1109/TITS.2018.2859765](https://doi.org/10.1109/TITS.2018.2859765).



**JIAN ZHOU** was born in Ningguo, Anhui, China, in 1995. He received the B.E. degree from the Department of Automotive Engineering, Harbin Institute of Technology, Harbin, China, in 2017. He is currently pursuing the master’s degree with the State Key Laboratory of Automotive Simulation and Control, College of Automotive Engineering, Jilin University, China.

His research interests include the path planning and trajectory tracking control of intelligent vehicles.



**QIAN SHAO** was born in Ningguo, Anhui, China, in 1995. She received the B.M. degree from the Department of Information Management and Information System, Nanjing Agricultural University, Nanjing, China, in 2017. She is currently pursuing the master’s degree with the Department of Management Science and Engineering, Business School, Jilin University, China.

Her research interests include deep learning and supply chain management systems.



**YULEI WANG** received the B.S. degree in physics from Nankai University, China, in 2008, and the Ph.D. degree in control science and engineering from the Harbin Institute of Technology, China, in 2013. During 2010–2012, he was a Joint Ph.D. Student with the Institute for Automatic Control and Complex Systems, University of Duisburg-Essen, Germany. In 2012, he joined the Autonomous Robots Lab, Chiba Institute of Technology, Japan, as a Visiting Scholar. From 2013 to 2017, he was a Lecturer with the Department of Control Science and Engineering, Jilin University, China. During 2018–2019, he held a postdoctoral position with the Institut fuer Regelungs- und Automatisierungstechnik, Graz University of Technology, Austria. Since 2017, he has been an Associate Professor with the Department of Control Science and Engineering, Jilin University.



**HONGYU ZHENG** received the B.E. degree in mechanical engineering and automation and the Ph.D. degree in vehicle engineering from Jilin University, Changchun, China, in 2003 and 2009, respectively.

From 2017 to 2018, he was a Visiting Research Scholar with the Department of Mechanical and Aerospace Engineering, The Ohio State University, Columbus, OH, USA. He is currently an Associate Professor with the State Key Laboratory of Automotive Simulation and Control, Jilin University. His research interests include vehicle dynamics and control, and control of autonomous vehicles.